

We are IntechOpen, the world's leading publisher of Open Access books Built by scientists, for scientists

6,900

Open access books available

185,000

International authors and editors

200M

Downloads

Our authors are among the

154

Countries delivered to

TOP 1%

most cited scientists

12.2%

Contributors from top 500 universities



WEB OF SCIENCE™

Selection of our books indexed in the Book Citation Index
in Web of Science™ Core Collection (BKCI)

Interested in publishing with us?
Contact book.department@intechopen.com

Numbers displayed above are based on latest data collected.
For more information visit www.intechopen.com



Flapping Wings with Micro Sensors and Flexible Framework to Modify the Aerodynamic Forces of a Micro Aerial Vehicle (MAV)¹

Lung-Jieh Yang
Tamkang University
Taiwan

1. Introduction

The flight of birds or insects has fascinated scholars and physicists for many centuries. Flapping motion, as shown by many nature flyers, is the most efficient way of flying objects whose size are smaller than or around 6 inches. In this chapter, the author introduced how to use modern technology to fabricate the flapping wings for micro aerial vehicles (MAVs) with flexibility and smartness. The terminology of MAV, defined by Defense Advanced Research Projects Agency (DARPA), denotes the size-limitation and the performance requirements of air vehicles (Ashley, 1998). The total wingspan of a MAV is expected to be less than 15 cm; the highest velocity is about 48 km/hr; the range of the flight mission is about 10 km; and the flight endurance is about 20-120 minutes.

The earliest flapping vehicle (or ornithopter) was made by Gustave Trouvé (Chanute, 1894). No ornithopter was developed using MEMS technology until the end of the last century. A lightest flapping MAV with a total mass of only 11.69 grams was made by Caltech micromachining lab in 1999-2002 (Pornsirak, 2001; 2002). They used titanium-alloy as the frame of flapping wings, and assigned parylene, a polymer material, as the covering skin of the airfoil. This integrated structure can withstand extreme vibration with frequency of more than 30 Hz and it weights only 0.3 gram. The Caltech MAV, "Micro-bat", can be remotely controlled as will and the flight endurance is more than 6 minutes. Besides the work of Caltech, several groups in other universities developed their flapping MAVs with different configurations and actuation principles (Website <http://www.artificialmuscle.com/>), (Website <http://fourier.vuse.vanderbilt.edu/cim/projects/crawler.htm>), (Website http://www.gtri.gatech.edu/atas/teams/proj_entomopter.html), (Sitti, 2001; Barrett, 2005; Jones, 2005). For instance, TU Delft's MAV "Delfly" composed of a pair of dragonfly-like flexible wings recently announced their successful hovering (Barrett, 2005). Otherwise, a

¹ The major content of this chapter is extracted from the author's following two papers:

L.J. Yang, C.K. Hsu, J.Y. Ho, and C.K. Feng, "Flapping Wings with PVDF Sensors to Modify the Aerodynamic Forces of a Micro Aerial Vehicle," *Sensors and Actuators A: Physical*, Vol. 139, pp. 95-103, 2007.

L.J. Yang, C.K. Hsu, F.Y. Hsiao, C.K. Feng, and Y.K. Shen, "A Micro-Aerial-Vehicle (MAV) with Figure-of-Eight Flapping Induced by Flexible Wing Frames," AIAA 2009-0875.

fixed-wing type MAV with a scissor-like clapping tail thruster made by Jones et al. of Naval Graduate School. They showed the long flight endurance over 20 min (Jones, 2005).

Although the previous interesting works of MAVs managed to fly via wireless remote control, none of the programs has been able to achieve a long and sustainable flight. Moreover, the detailed mechanism of the flapping flight is still under study and the unsteady aerodynamic characteristics of the flapping MAVs are unclear.

Predicting the lift force during flight is a very critical issue in the design of a MAV. Measuring the instantaneous aerodynamic force on a flapping model or live insect remains a great challenge in experimental aerodynamics. The early surveys of measuring averaged force were made using delicate balances (Hollick, 1940; Jensen, 1956). Other prior researches used piezoelectric probes (Cloupeau, 1979), strain gauges (Ho, 2003) and the laser interferometers (Dickinson, 1996). Restricted by the size of measuring tools, it is usually assumed that all the wings behave identically and have the equal force contribution to the flying body. Therefore, efforts should be focused on fabricating the very dedicate and identical wing structures in the conventional development of MAV.

In order to gather more information during the flapping maneuver, we measured the aerodynamic force of a Caltech-like MAV by the conventional load-cells in the wind-tunnel, and also proposed the integration of PVDF piezoelectric foils to the parylene flapping wings of the MAV to pick up the *in-situ* lift force. We used MEMS technology to fabricate a titanium-alloy wing frame and a set of gear-reduction transmission components, and deposited conformal parylene film on the wing frame as the airfoil skin (Pornsin-sirirak, 2001; 2002) (Website <http://parylene.com>). The actuation force or torque available for the flapping wings is drained from the gear-reduction transmission set coupled to a high-speed DC motor powered by commercial poly-lithium batteries. The parylene wing skin also serves as an electrical isolation layer between the PVDF piezoelectric sensing element and the titanium frame. The on-site lift information acquired from a PVDF sensing skin was done by the authors of this presented work. Herein, we employed four-linkage concept to design a transmission mechanism for the MAV. Although the two wings of the MAV have the same flapping angle, there exists unavoidably a mechanical phase lag between them by virtue of the transmission's mechanical principle of operation. The result in this chapter proposes a novel approach of integrating a parylene-PVDF hybrid wing in an *in-situ* way to monitor the lift force of a flapping MAV in the wind-tunnel test. We found a new design methodology to adjust the aerodynamic performance of MAV by changing the phase lag between the two flapping wings through fine tuning of the mechanism linkages.

Additionally, the figure-of-eight stroke of hovering hummingbirds is the ideal trajectory which many researchers of flapping MAVs hope to pursue. Several sophisticated mechanisms of flapping wings were claimed to fit this natural maneuver motion in the conceptual design, for instance, the Banala et al. in Delaware University employed a 5-bar mechanism for generating a prescribed wing motion taken from hawkmoth kinematic flight data (Banala, 2005). They designed a mechanism for biaxial rotation of a wing for a hovering MAV (McIntosh, 2006). Meanwhile, an insect-like flapping wing mechanism was proposed by Cranfield University (Żbikowski, 2005; 2005) through the novel idea of a double spherical Scotch yoke. All the above designs have still not availably been applied to the 20-cm size MAV and there exists scarcely successful examples of this kind artificial palm-size MAVs manufactured by conventional machining. Herein, a biomimetic figure-of-eight flapping induced by the flexible wing frames of the MAVs in this chapter were found accordingly.

The flight information obtained from a MAV with successful flight record can be as a reference compared to natural flapping animals, and give a guideline to the development of next generation MAV in an empirical manner.

2. DESIGN CONCEPT

The issue of reducing weights for an air vehicle, especially for a flapping-wing flight vehicle herein discussed in this chapter, is a very critical problem. The current trend is to employ small, palm-sized wing foils. However, lift and thrust forces produced by the movement of wing flapping also decreased with size reducing of the airfoil, and therefore the wing size should be sufficiently large. For this reason, adopting the titanium-alloy of high strength-to-mass ratio as the airframe material and parylene as the skin material of flapping-wing is an appropriate compromise. Note that a light-weighted and high-power battery is also needed. To obtain an accurate size of a titanium-alloy airframe with no residual stress is not easy with the conventional machining methods. Interior residual stress could cause a warping deformation in the structures of airframes, and easily distorts the geometry of the airfoil. Therefore, instead of the regular machining techniques, wet etching technique is employed to tailor the airframe structures from a titanium-alloy plate and no apparent residual stress is found. Parylene coating technique is applied to laying the wing skin attached on the titanium frame. The followings are the design details of the airframe and a gear transmission system associated with the airframe.

2.1 Design of the titanium-alloy airframe

The flapping-wing movement of a nature bird includes flapping, twisting, folding and gliding. These functions correlate to the high efficiency of flapping mechanism. In order to reach very light weight, the MAV in this work has flapping movement of only one degree-of-freedom on purpose. Therefore in order to achieve better flight performance, the flapping wing must be able to sustain higher flapping frequency and provide sufficient force for flight. Higher flapping frequency involves concerns with the structural integrity. Designing the flapping wings with high strength and low weight is a crucial issue.

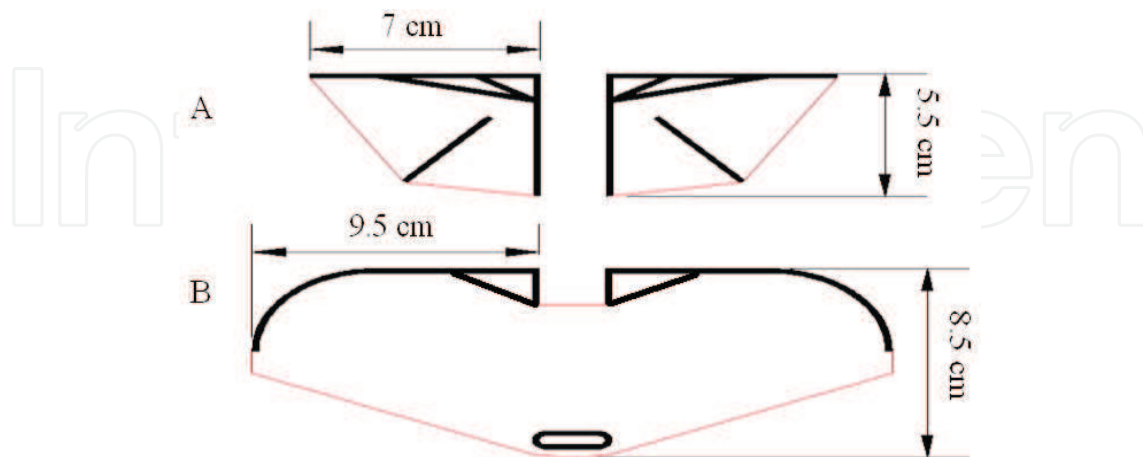


Figure 1. Two types of flapping-wing frame in which the thickness of Ti-alloy frame is 250 μm and 2 mm in width, and the areas of Wing A and Wing B are 64.50 cm^2 and 108.75 cm^2 , respectively

We use existing MEMS technology for fabricating the wings to ensure the accurate size control and smartness of the flying system. The material of the airframe is titanium-alloy (the mechanical properties of titanium grade 4: density = 4.54 g/cm³; Young's modulus = 104 GPa; tensile strength = 552 MPa). The detailed dimensions of two types of the flapping wings as well as their wing frames are shown in Fig. 1.

2.2 Design of the gear transmission system

The gear transmission system for the MAV is composed of a gear-reduction set and a four-bar linkage, as shown in Fig. 2. We use a 7mm-diameter DIDEL electric motor to drive the transmission system. The gear set with a gear ratio of 26.6 adopted in this work provides a sufficient torque for driving the flapping wings. The whole gear set and the motor are arranged on an aluminum base. OA is the driving linkage and the following linkage BC is connected to the wing structure. The driving linkage can perform a full revolution and the following linkage undergoes a rocking motion. The links OA, BC are made of aluminum by EDWC (electrical discharge wire cutting) (Weller, 1983), and the link AB is made of titanium-alloy by MEMS process. The nodal point is a 1mm-diameter stainless tube that connects the aluminum base rigidly.

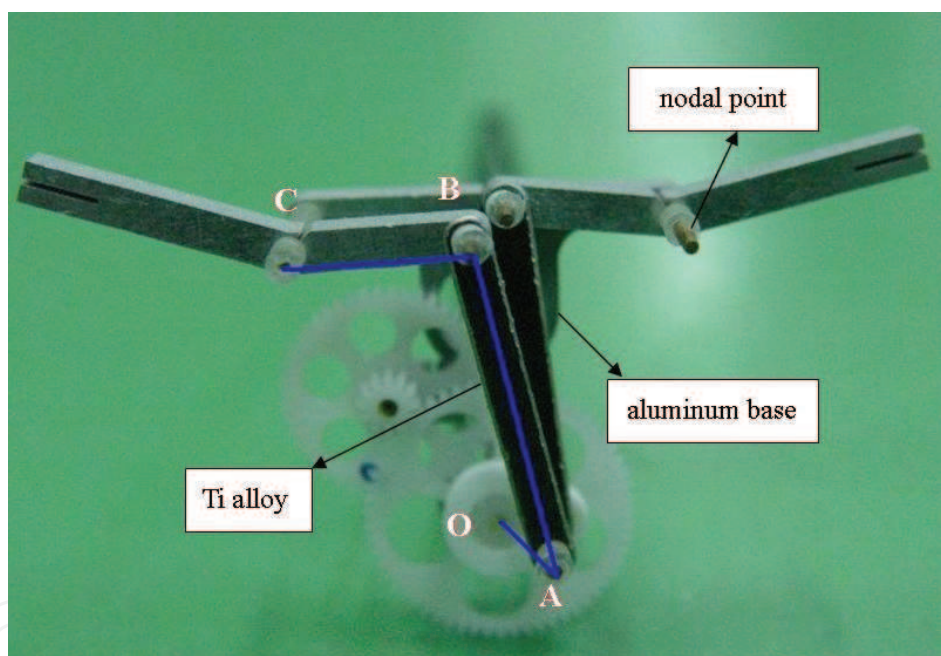


Figure 2. Gear transmission system. In wind-tunnel tests, the aluminum base is adopted and the light plastic base is selected for real flight

We can easily achieve different stroke angles and flapping symmetry (the lag phenomenon between the two wings in the flapping motion) by adjusting the dimensions of links OA, AB and BC. The selected lengths for each links are OA=4 mm and AB=21.5 mm. Link BC has a variable length, which varies from 8 mm to 12 mm, and with length variation of such a range, there are correspondingly large changes of stroke angles and phase angle lags (max) in flapping movement, as seen in table 1. Although the two wings have the same flapping angle of 39 to 61 degrees, there exists unavoidably a mechanical phase lag of 2.5 to 13 degrees between them due to the gear-transmission's principle of operation (see the simulated data in Fig. 3.)

BC (mm)	Stroke angle (degree)	Lag (max)
8	60.5	13.3
9	53.0	9.4
10	47.2	6.4
11	42.7	4.1
12	39.0	2.5

Table1. Designs of the transmission system

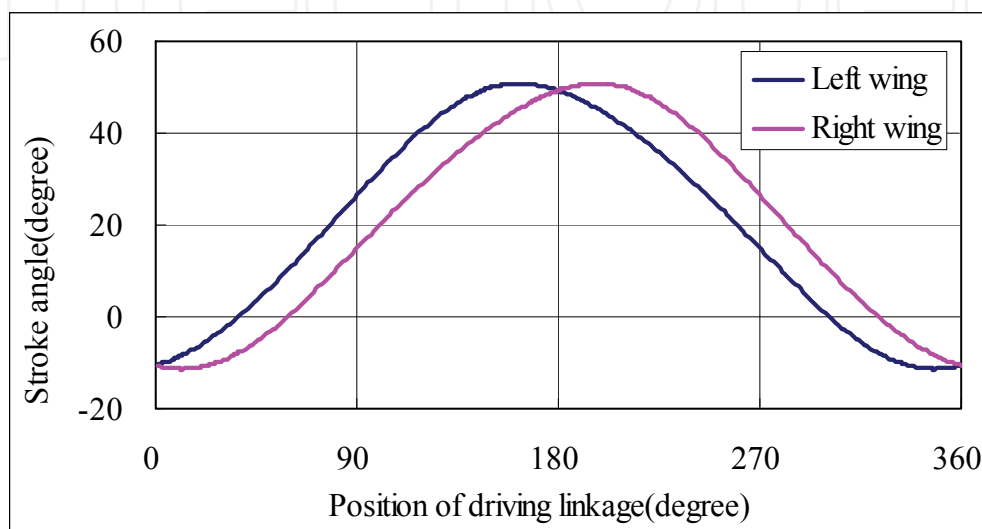


Figure 3. Stroke angles of two flapping wings vs. one period of time

2.3 Aerodynamic force measurement by PVDF

Piezoelectric materials have been widely used in many key technologies, including microelectronics, signal processing, sensors and actuators. Among all piezoelectric materials, the PVDF material can be fabricated in any shape of thin film and integrated with parylene by MEMS technology. Thus, a flexible thin film of PVDF is suitable in studying the aerodynamic force of flapping wings.

The mathematical model for lift force measurement by PVDF is described as follows. We assume that there is a pressure difference distribution $\Delta p(x,y,z)$ between the upper and the lower sides of the flapping wing. Lift force is calculated by taking the integral of Δp over the wing surface S :

$$L = \iint_S \Delta p(x, y, z) dA \tag{1}$$

When the pressure difference Δp of the air flow field acts on the PVDF film, just like the case of giving a force on a shell or a plate, the PVDF film and wing skin become deformed and stretched. We assume the plane stress distribution on the flapping wing is $\sigma_x(x,y,z)$ and $\sigma_y(x,y,z)$ which are related to $\Delta p(x,y,z)$ by the following linear relationship (Hooke's law):

$$\Delta p(x, y, z) = k_x(x, y, z) \cdot \sigma_x(x, y, z) = k_y(x, y, z) \cdot \sigma_y(x, y, z) \tag{2}$$

where k_x and k_y are stiffness functions assumed by the authors. Regarding PVDF film as an air foil for sensing aerodynamic force, we get the charge density ρ_i ($i=x,y,z$) by the following piezoelectric transformation relationship (Liu, 2006):

$$\begin{bmatrix} \rho_x \\ \rho_y \\ \rho_z \end{bmatrix} = \begin{bmatrix} 0 & 0 & 0 & 0 & 0 & 0 \\ 0 & 0 & 0 & 0 & 0 & 0 \\ d_{31} & d_{32} & d_{33} & 0 & 0 & 0 \end{bmatrix} \begin{bmatrix} \sigma_x & \sigma_y & \sigma_z & \tau_{xy} & \tau_{yz} & \tau_{zx} \end{bmatrix}^T \quad (3)$$

The none-zero coefficient d_{ij} of PVDF film are

$$\begin{cases} d_{31} = 20 & pC/N \\ d_{32} = 2 & pC/N \\ d_{33} = -30 & pC/N \end{cases} \quad (4)$$

We assume the flapping wing as a plane-stress problem, ($\sigma_z=0$). The charge density along the Z-direction therefore can be derived as:

$$\rho_z(x, y, z) = d_{31} \cdot \sigma_x(x, y, z) + d_{32} \cdot \sigma_y(x, y, z) \quad (5)$$

Combining Eqs. (2 to 5), we get the total charge Q in terms of the pressure difference Δp and the stiffness function k as follows:

$$Q = \iint_S \rho_z(x, y, z) dA = \iint_S \Delta p(x, y, z) \cdot \left[\frac{d_{31}}{k_x(x, y, z)} + \frac{d_{32}}{k_y(x, y, z)} \right] dA \quad (6)$$

Because the stiff function k_x and k_y are not uniform over the wing skin area S , the lift force L in Eq. (1) can not be directly separated from Eq. (6). We temporarily and equivalently replace the bracket in Eq. (6) with d^* , and obtain the following expression:

$$Q = d^* \cdot L \quad (7)$$

In Eq. (7), the total charge Q can be also expressed by a voltage V across the piezoelectric (PVDF) capacitor C by the relationship

$$Q = C \cdot V \quad (8)$$

Combining Eqs. (7) and (8), the lift force can be determined linearly with the voltage V .

$$L = \frac{Q}{d^*} = \left(\frac{C}{d^*} \right) V \quad (9)$$

The simplified model described by Eq (9) gives us a guideline in principle that the lift information can be obtained electrically from the voltage given by the PVDF piezoelectric film in an *in-situ* way. In addition, such an output signal from the PVDF film needs calibration or quantitative comparison with the load-call sensors installed in the wind-tunnel available for the test of MAVs in this work.

3. FABRICATION

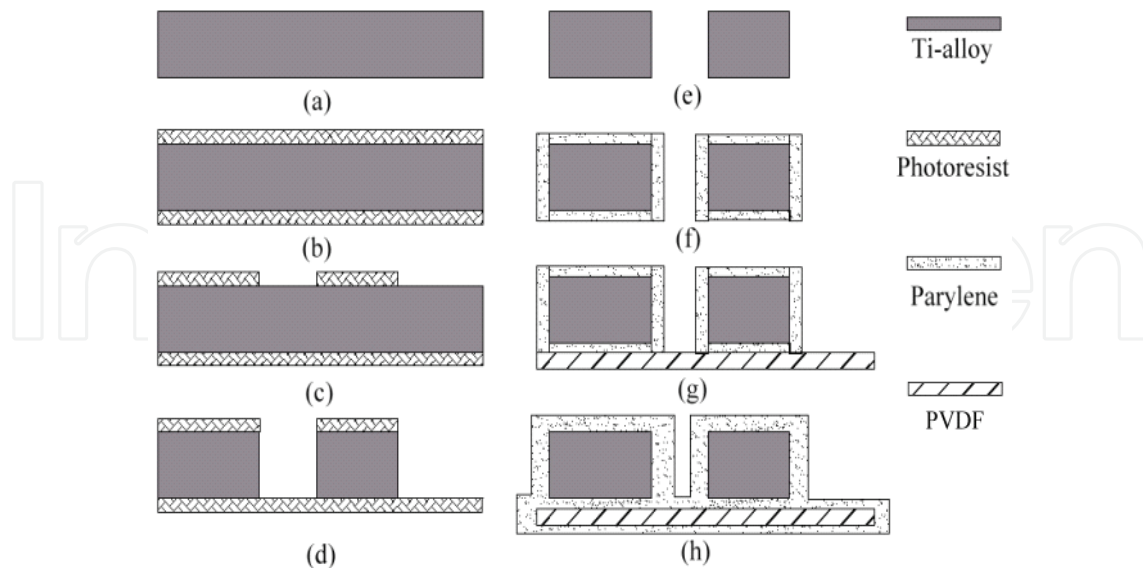


Figure 4. Process flow of a PVDF-parylene wing : (a)Clean the titanium-alloy substrate; (b)Coat the double sides of the titanium-alloy substrate with photoresist (PR); (c)Photolithographically pattern the PR on the top side as the etching mask; (d) Etch the titanium-alloy substrate to wing frames by HF acid; (e)Strip PR and clean; (f)Coat the first parylene film as the insulated layer; (g)Paste titanium-alloy frame with PVDF; (h)Coat the second parylene film all over the PVDF and wing-frame, and complete PVDF-parylene wings

The fabrication process of titanium-alloy MEMS wings with sensing PVDF film is shown in Fig. 4 and described as below.

- Step (a): A titanium-alloy substrate is cleaned with acetone and isopropyl alcohol (IPA). Then, it is flushed with de-ionized water (DI water.)
- Step (b): Both sides of the titanium-alloy substrate are coated with photoresist (PR), AZ4620, by a spin coater. Exact control of the rotation speed is exercised to get 10 μm thick PR, serving as a mask layer for subsequent operation.
- Step (c): The upside PR is patterned by an I-line UV contact aligner. This step defines a pattern as an etching masking for the titanium-alloy frames against chemical etchant. The developer for the AZ4620 PR is AZ400K.
- Step (d): The titanium-alloy substrate is dipped in hydrofluoric (HF) acid to etch uncovered titanium for 50 minutes. After the etching process, the geometry of the wing frames appears.
- Step (e): The substrate then put in acetone solution to strip PR from both sides of the titanium-alloy substrate. All the parts are cleaned and flushed with DI water.
- Step (f): The first parylene diaphragm is deposited on the titanium-alloy in the SCS PDS-2010 parylene coater. For this step, 15 g of parylene dimmer yields an approximately 11.5 μm thick film and this parylene film is used as an insulated layer.
- Step (g): A 25 μm thick piezoelectric film, PVDF, is pasted on the frames.
- Step (h): The PVDF film and the wing frame are coated with the second parylene layer.

Having done the process mentioned above, we can get the PVDF flapping wings shown in Fig. 5. The parylene flapping wings without PVDF sensing film are obtained by the similar process, except using another pasting tape as the supporting stuff in Step (g) and

delaminating the tape after parylene coating. By careful fabrication and assembly, two types of MAVs in this work are shown in Fig. 6. The two-wing MAV named Wing A (Caltech-like MAV) has a mass of 7.91g, whereas the single-wing MAV Wing B has a mass of 7.52g. The total mass of the two MAVs are increased to 13.91 and 13.52 grams respectively after they are combined with empennage and poly-lithium batteries additionally.

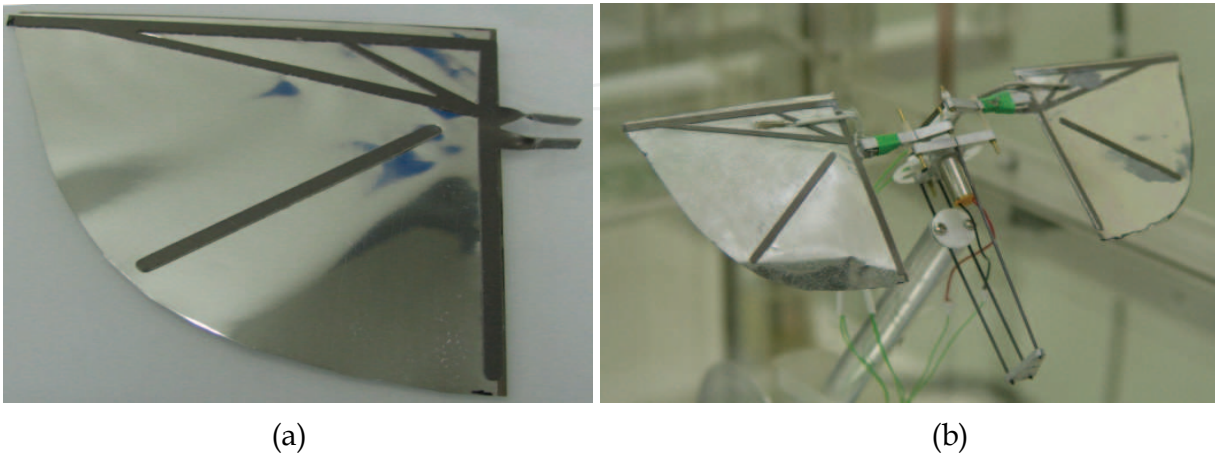


Figure 5. MAV models in wind-tunnel: (a) The completed PVDF-parylene flapping wing. (b) Setup for testing the flapping wings with PVDF sensing skin in the wind-tunnel

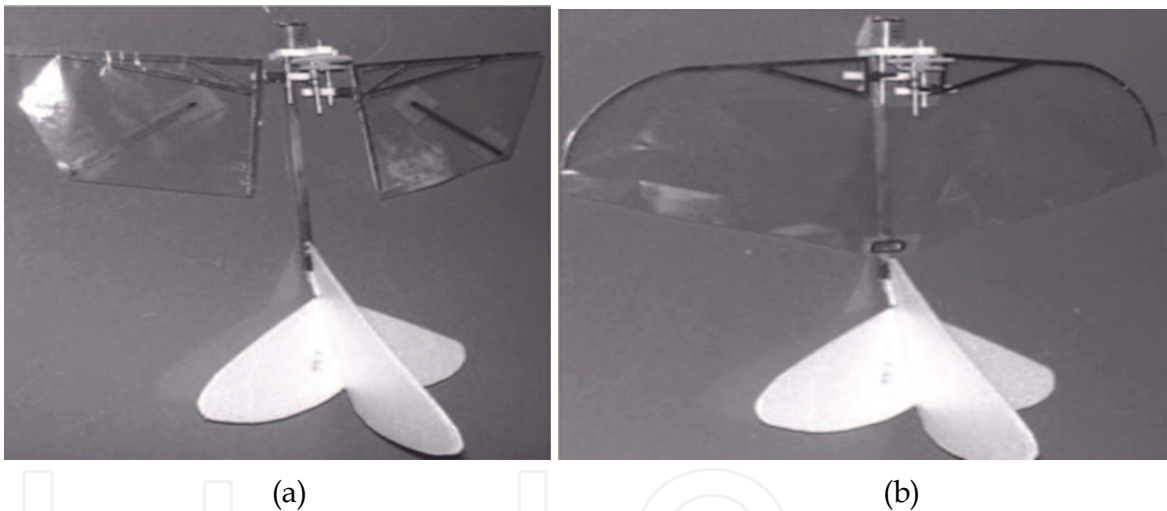


Figure 6. The appearance of the flapping MAVs (including gear transmission system, wings, DC motor, fuselage, and tail): (a) Wing A with mass of 7.91 g; (b) Wing B with mass of 7.52 g

4. TEST AND RESULTS

4.1 Wind-tunnel test

The aerodynamic testing of MAVs in this work was conducted in a small wind-tunnel. The dimension of the test section has a space of $30 \times 30 \times 100 \text{ cm}^3$ and the inlet contraction ratio is 6.25. The wind speed ranged from 0 to 7 m/s, measured with a hot-wire anemometer. The load-cell (Bertec, OH, USA) with specifications of 200 g and 100 g are responsible for the force measurement of lift and drag, respectively. It has the maximum error 0.2% of the full-scale signal due to the linearity or hysteresis. In the wind tunnel testing, the MAV is placed on the load-cell directly to obtain the data of lift and drag forces. Fig. 7 shows the experimental setup.

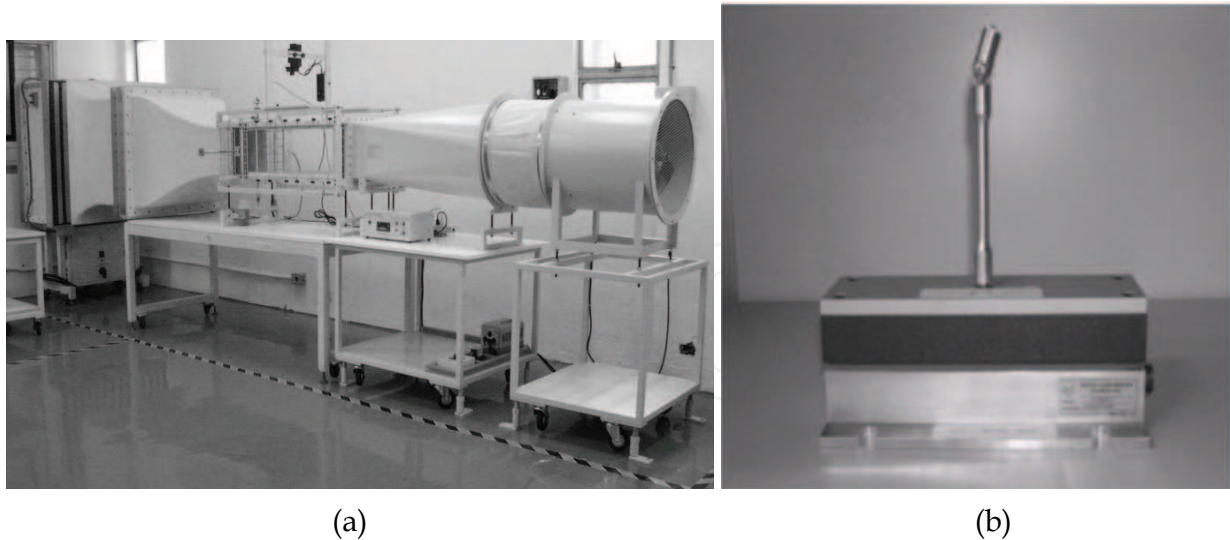


Figure 7. The wind-tunnel test system: (a) Low speed wind-tunnel; (b) Load-cell (Bertec Corp.)

The scheduled process of collecting a data point by the setup in Fig.7 is defined as below:

1. 0 s: Turn on the load cell;
2. 2 s: Reset the load-cell;
3. 5 s: Turn on the wind-tunnel;
4. 12 s: Start the flapping of the MAV;
5. 18 s: Start the data collection of lift and thrust;
6. 30 s: Stop the data collection (the total data collection time is 12 s.)

The data-breeding rate of the load-cell is set as 1,000 points per second. Then we collected 12,000 points of data in every flapping condition, and integrate them into time-averaged values of lift L and thrust T . These 12,000 point data may not be divided into round number of cycles for different wingbeat frequencies (from 7.2 to 23.6 Hz). However, the error due to noninteger cycles of wingbeating is confined less than 0.47 %.

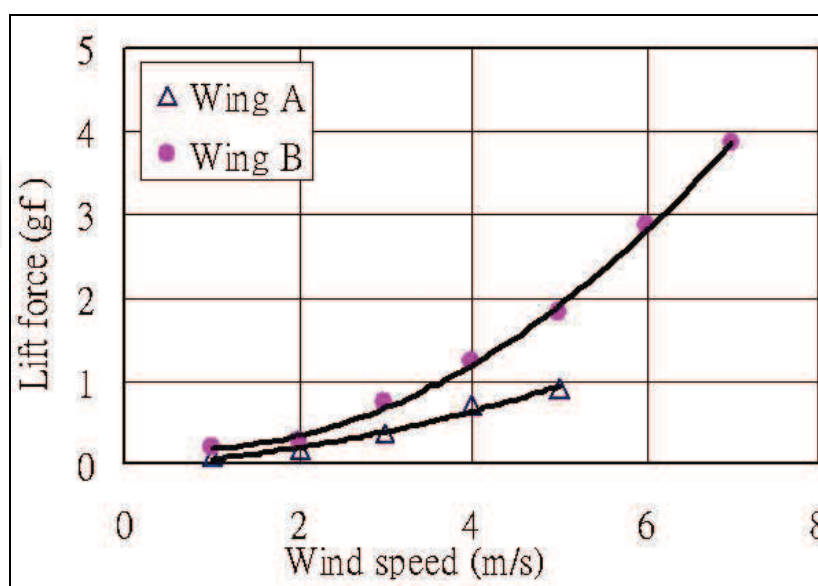


Figure 8. Relationship of lift-force vs. wind speed with no flapping

In order to study the relationship between the lift force and the wind speed. The MAVs with parylene wings are set at an attack angle to 20 degrees. Wing A and Wing B were measured successively with no flapping in the wind-tunnel first. With wind speed increased from 1 to 7 m/s, the lift force increase vigorously. The acquired data of lift force versus wind speed are shown in Fig. 8. This result reveals that Wing B has a greater lift force than Wing A (Caltech-like) does due to the larger wing area. Both of them have the right tendency that lift forces increase with the square of wind speed.

The aerodynamic performance of the two wings during flapping was also studied. In the flapping test, the flapping frequency f is controlled by a DC motor and the voltage applied to the motor was set from 3 V to 7 V to get the flapping frequency ranging from 7 Hz to 16 Hz. This dynamic experiment was conducted at the wind speed U of 1 to 5 m/s. Fig. 9 shows the experimental results. The lift and thrust coefficients can be expressed as follows:

$$C_L = \frac{2L}{\rho \cdot A \cdot U^2} \quad (10)$$

$$C_T = \frac{2T}{\rho \cdot A \cdot U^2} \quad (11)$$

where L, T, ρ, U , and A are lift, thrust, air density, flight speed, and wing area, respectively. The advance ratio J is also defined as the ratio of the flight speed to the speed of the wingtip:

$$J = \frac{U}{2 \cdot \phi \cdot f \cdot b} \quad (12)$$

where ϕ, f and b are stroke angle, flapping frequency, and semi-wing span, respectively. For the general case of unsteady-state flapping flight, the advance ratio J is less than 1. The advance ratio J approaches very large for the case of a fixed wing (no flapping). In this work, even with a constant angle of the attack is set constant (20 degrees), we can still adjust the flapping frequency and the wind speed to get various values of J in the flapping (dynamic) test. From the result illustrated in Fig. 9, in the regime where J less than one (unsteady state) the C_L is increased rapidly. With J increasing, the C_L approaches to the static value of 0.1 ($J > 4$) which is almost equal to the value of C_L of no flapping mode in Fig. 8.

The result of Fig. 9 also shows that Wing A (Caltech-like MAV) is superior to Wing B both in generating lifts and thrusts during the flapping flight. The data are rather scattering near $J=1$. The issue is due to the very long testing time (over 10 hours for extracting 50 data points of C_L and C_T) of our MAV in the wind tunnel. Consequently, the structure of our MAV encounters the aging problem. For example, many mechanical components of the MAV start to deviate from their original positions, and consequently degrading their aerodynamic performance. Fig. 9 also reveals that, as J is less than 1, Wing A (Caltech-like) generates somewhat larger lift and thrust coefficients than Wing B in the flapping mode of flight. It is for the excuse that Wing A has its wing spar, wing chord and wing rib stronger than Wing B, and such a high stiffness of flapping wing generates flight with high speed and flapping frequency.

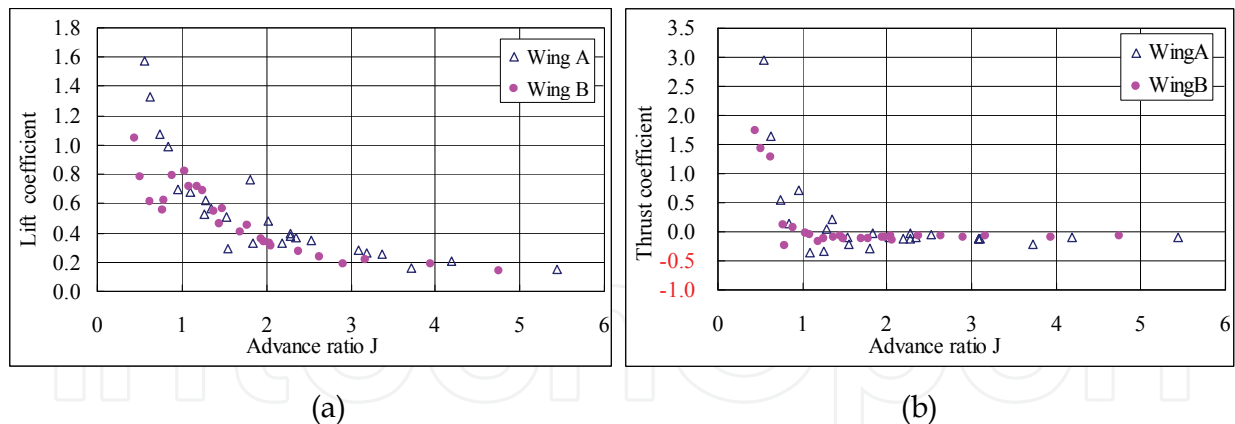


Figure 9. The unsteady aerodynamic characteristics of Wing A and Wing B. (a) lift coefficient ; (b) thrust coefficient

We also allowed the two types of flapping MAVs to perform their free flights, i.e., let them sustain the flight by poly-lithium batteries without remote flight control on the stability of the MAV in real time. Even though Wing A has a superior aerodynamic performance as mentioned above, it is hard to have a successful free flight. The reason may be due to that the difficulty in locating and adjusting the gravitation center as well as the aerodynamic center of this two-wing MAV that we cannot ensure the static stability of the Wing A (Caltech-like). On the contrary, Wing B has a successful free flight with a flight range of more than 10 meters.

The on-site lift output from PVDF sensing skin on the MAV is no doubt the primary viewpoint and contribution of this work. The Wing A with PVDF-parylene composite skin is adopted for this test. The aerodynamic signals are picked up successfully by PVDF and load-cell simultaneously. While the link BC is 11 mm, the collected lift data are shown in Fig. 10. It appears that there is a phase delay between the PVDF signal (Fig. 10(a)) and load-cell signal (Fig. 10(b)). However this is due to that the left wing is composed of a PVDF sensing skin and the right wing is pure parylene. The signal from the PVDF film denotes the lift information of the left wing, which does not include that of the right wing. Meanwhile, the signal from the load-cell sums up the global forcing effect from both wings. With variable lengths of link BC, the phase lag of the two wings resulted in the curve of PVDF, which is ahead or behind the load-cell.

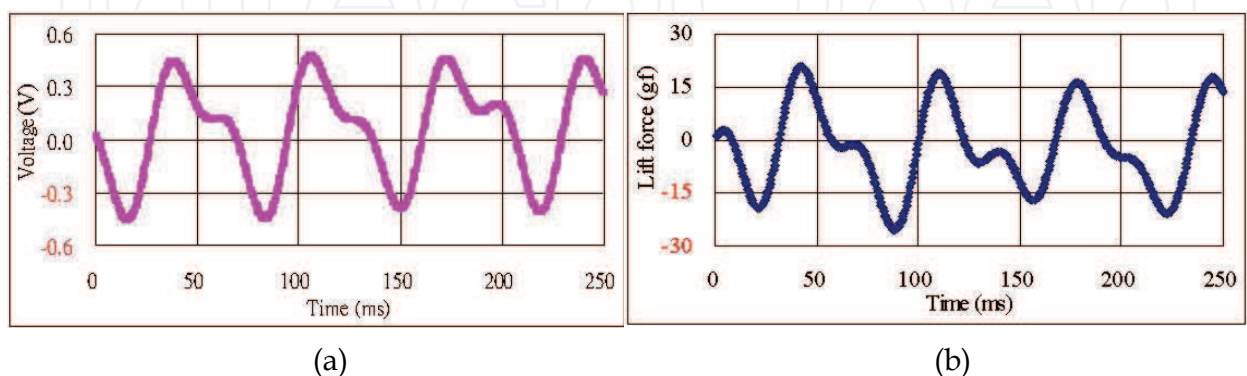


Figure 10. Lift signals of the MAV: from (a) PVDF film and (b) load-cell

By superimposing a similar curve of Fig. 10(a) with a proper phase lag (11 degree) into Fig. 10(a) itself, we can get the “pseudo” result in Fig. 11 which matched with Fig. 10(b) very well in a qualitative way. To arrive at the proper phase lag for superimposition, we accurately superimpose by mathematical method, from 0 to 27 degrees, and use the standard deviation to define the similarity between the pseudo PVDF and load-cell curve. We find the phase lag of 11 degrees is the most fitting case, as shown in Fig. 12.

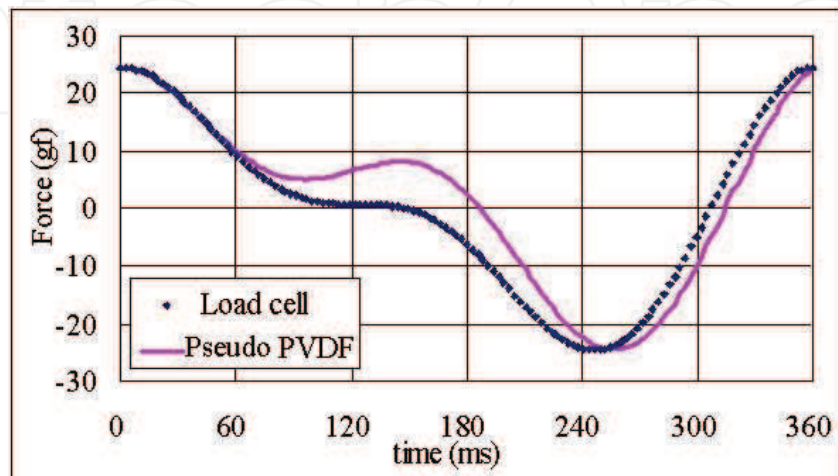


Figure 11. The “pseudo PVDF” signal comes from superimposing a similar curve of Fig. 10(a) with a proper phase lag (11 degree) into Fig. 10(a) itself to match well with load cell signal

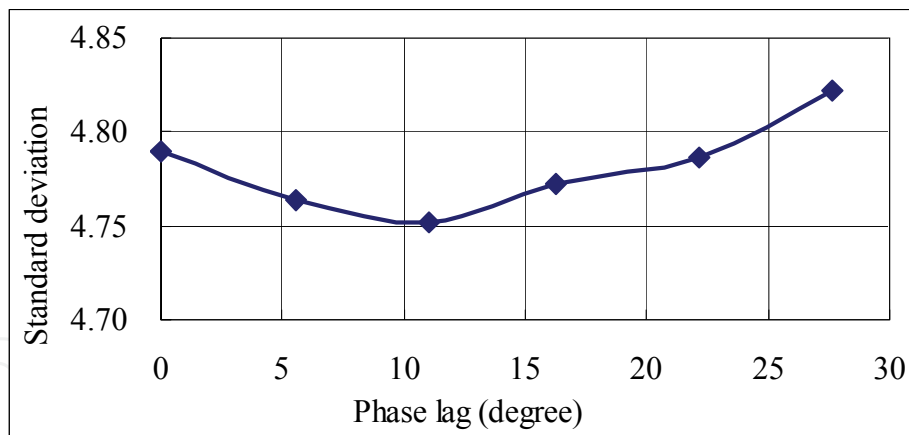


Figure 12. By using the standard deviation to judge the similarity

One of the significant findings from the new configuration of the flapping wings is that the phase lag of the gear transmission system is inevitable in the mechanical design. Therefore it is instead used to enhance the lift behavior of MAV. For example, we can make the lift curve smoother to sustain a better attitude of the MAV during the flapping cruise. After establishing the relationship between the phase lags from gear-transmission and the lift response in Fig. 13, we will adjust the aerodynamic performance of MAV reliably by changing the phase lag between the two flapping wings through fine tuning the mechanism linkages of the gear transmission system.

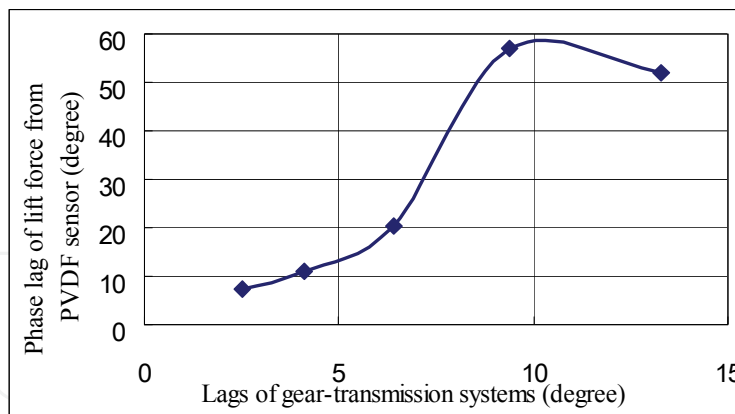


Figure 13. Deduced phase lag of lift force from the PVDF sensor vs. different lags of gear-transmission systems

4.2 Improved flight performance

Based on the experience of the preceding free flight tests of MAVs, we found two problems influencing the flight performance. First, the transmission system needs two poly-lithium batteries of 6.5 g weight to supply the power for sustaining the wing flapping with a frequency of 16Hz. The weight of the batteries is a critical issue since they contributed half of the MAV's total weight. The second issue involves the un-balanced angular momentum which yields the shaking phenomenon from the gear transmission system. It will alter the attitude of the MAV and result in a disastrous flight consequence, such as stall.

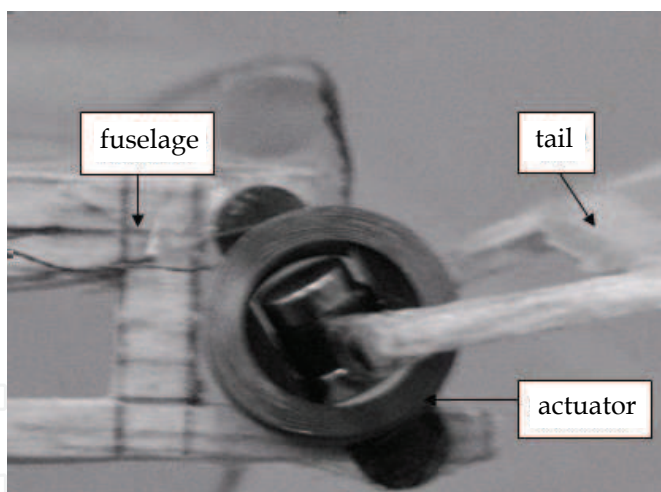


Figure 14. The actuator connects the fuselage and the tail

In order to get a desired flight via wireless control on purpose, light weight materials for the components of the MAV and re-design of the gear transmission system is required. We set the length of wingspan to be 30 cm and 8 cm in wing cord and there is no rib placed in the airfoil. By utilizing the previous fabricating experience of MAV, the new acrylic base as well as the gear transmission system that has a gear ratio of 26.6 is installed. In addition, light receiver and a magnetic actuator which are only 0.9 g and 1.1 g, respectively are employed in the MAV as well. The receiver has two channels, one to control the rotating speed of the DC motor and the other to adjust the tail actuator acting as a rudder for airplanes. In order to match the actuator on purpose, the construction design of the fuselage and the tail actuator is shown in Fig. 14.

Finally, we integrate all the components including the receiver for the remote control, tail, actuator, and one poly-lithium battery into the MAV. The total weight of MAV is 10.67g. The MAV named as “Eagle-II” is shown in Fig. 15. In the flight testing with wireless attitude control, the MAV has a successful flight with a range of 40 meters and an endurance of 10 seconds. The detailed flight trajectory of the MAV prototype is shown in Fig. 16. We additionally measured the averaged aerodynamic data of “Eagle-II” and shown in Fig. 17.

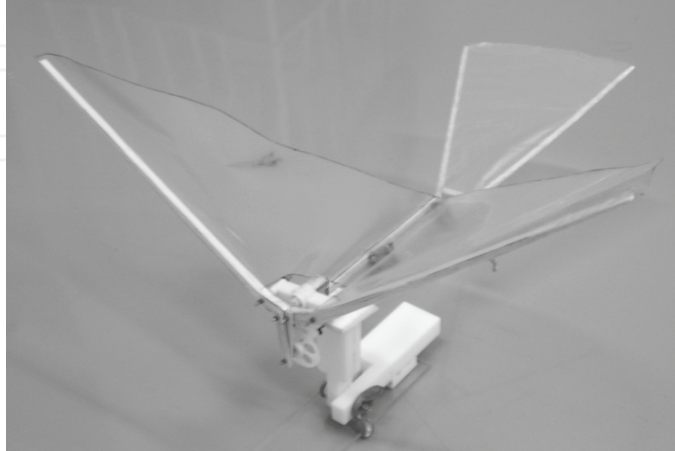


Figure 15. The appearance of modified MAV “Eagle-II” with the configuration of Wing B

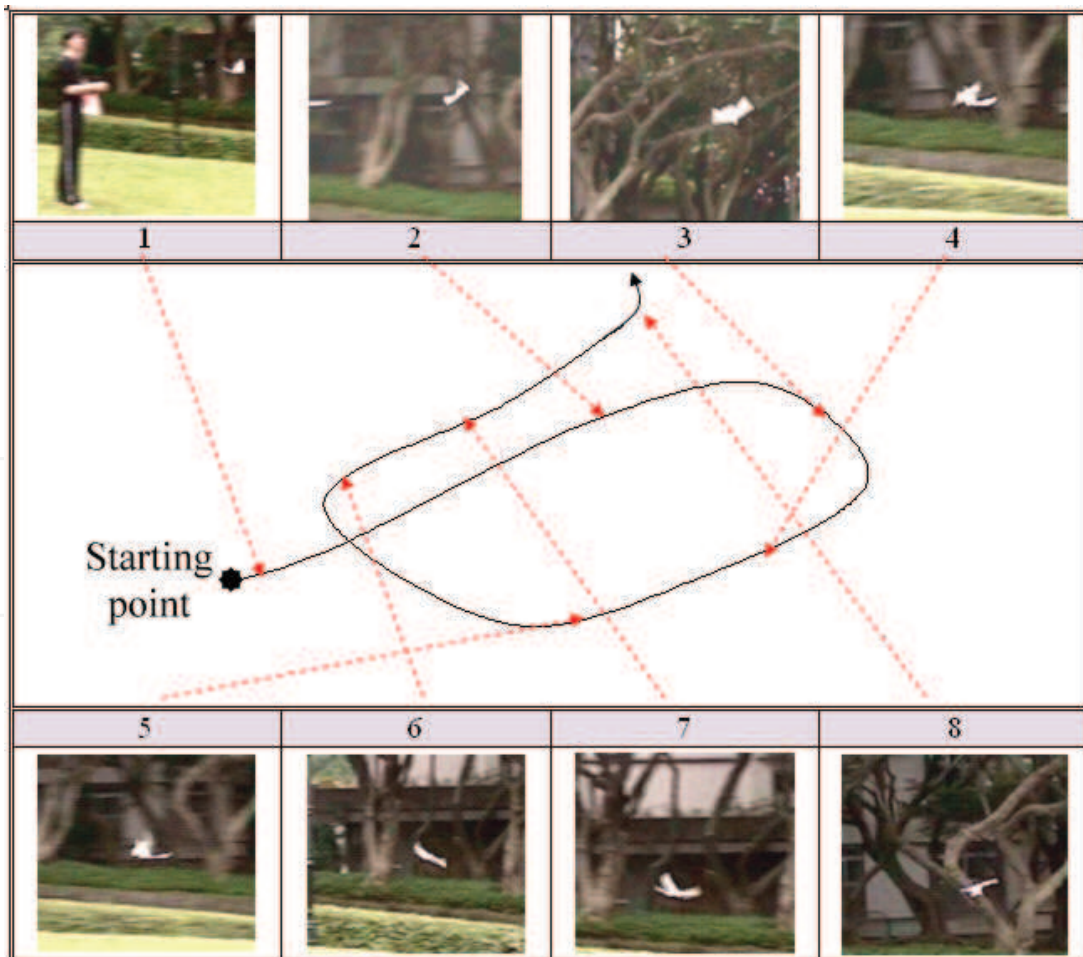
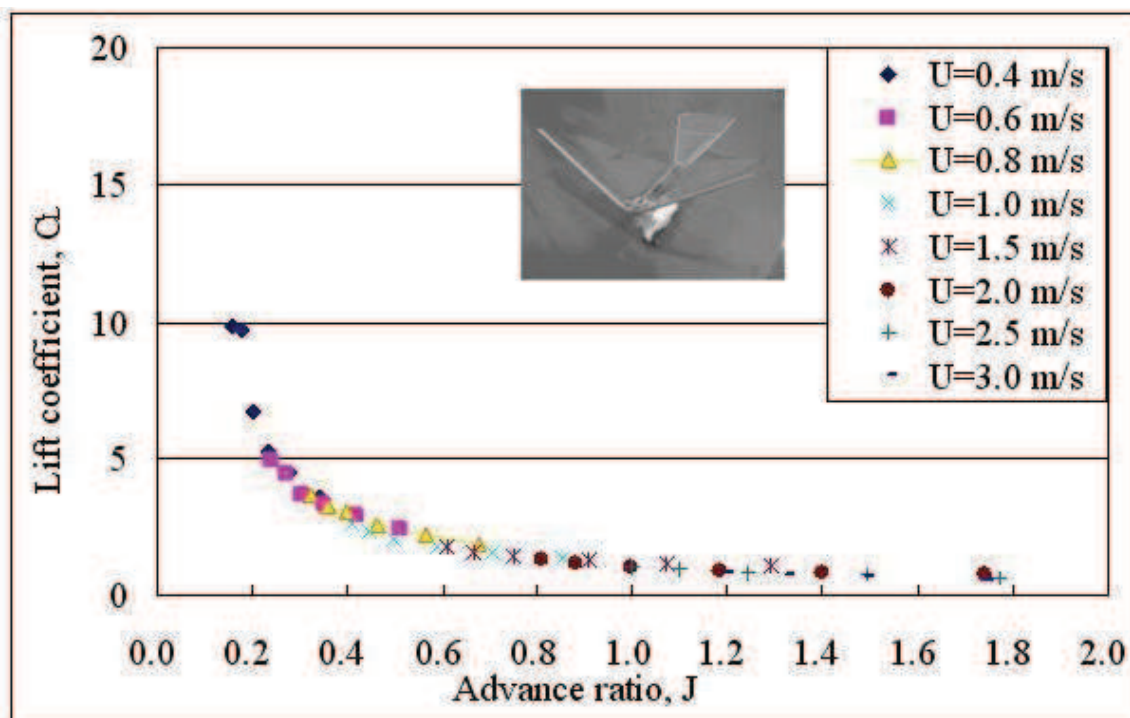
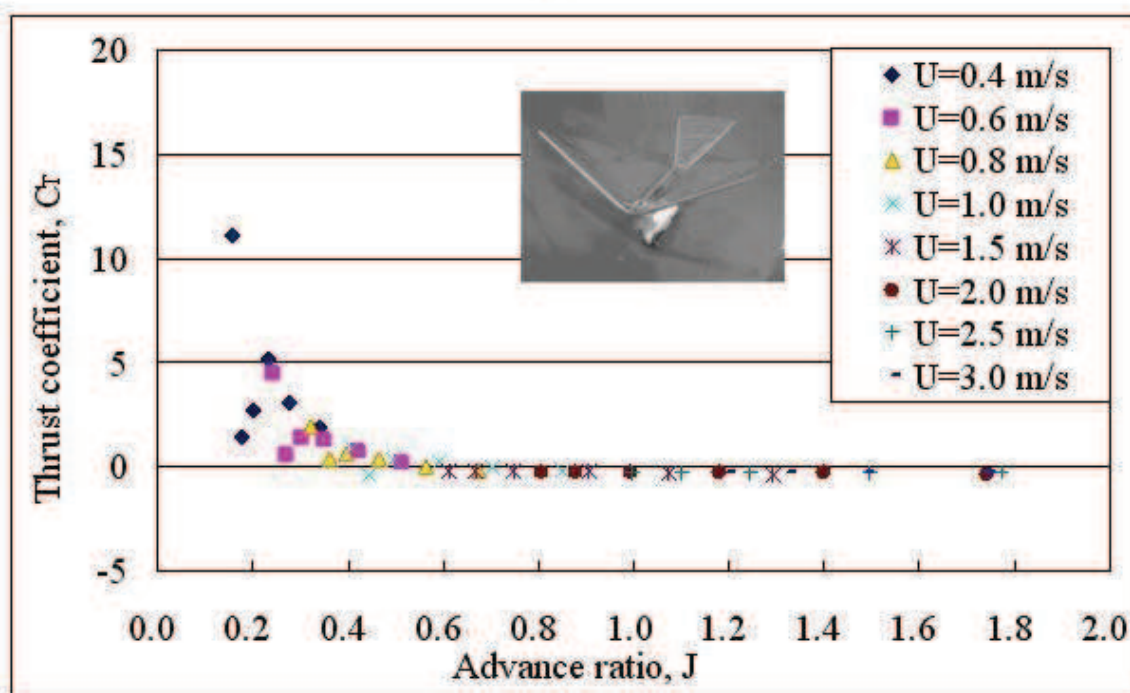


Figure 16. The flight trajectory of MAV



(a)



(b)

Figure 17. (a) Lift coefficient C_L and (b) thrust coefficient C_T of the MAV "Eagle-II" versus advance ratio J corresponding to different freestream velocities U . The wing skin of the assembled MAV "Eagle-II" has been changed as parylene film of 20-30 μm thick, and the leading edge beam is made of Balsa wood and it is quite stiffened compared to wing skin

4.3 Modification of MAVs

The flapping stroke angle ϕ is set as 35° for the case of "Eagle-II". It is really small compared to the stroke angle of 120° for hummingbirds (mentioned in the book of Norberg (Norberg, 1990)) or even the case of 60° or more for other medium-size birds. This angle limitation of our MAVs is due to the considerations of light weight and wear capability for the four-bar linkage module.

The lift and thrust coefficients C_L , C_T are extracted from a wind-tunnel test of the MAV "Eagle-II" with a semi-rigid leading edge subject to a fixed inclined angle of flapping plane of 20° (larger than the ordinary stall angle-of-attack 15° for the fixed-wing planes) and different advance ratios. Of course, the actual instantaneous angle of attack for the flapping flyers may be changing with time and larger than 20° . Even highest angle amplitude of attack, e.g., 50° , for the unsteady cases still does not cause catastrophic flow separation or stall, rather induce better unsteady lift force by paying the price of smaller thrust. This is the famous effect termed as "delayed stall"¹³. In general, these time-averaged lift coefficient C_L of the MAV larger than 3.0 in the regime of J below 0.4 resembles the enough counterbalance force to the weight of the MAV. The thrust coefficient C_T subject to J value below 0.4 is always positive also denotes the continuous forward pushing without speed decreasing during the real flight.

However, after a certain period of operation time the thrust data in the small advance-ratio or high flapping-frequency region reveal the trend of diversity or data fluctuation. Such a diversity of thrust data was traced back and suspected from the irregular operation of the worn gear transmission module. In other words, the wear of the power transmission mechanism impedes the smooth flapping and induces the corresponding unpredictable aerodynamic forces. Figure 18 shows the detailed four-bar (black dash line) gear transmission module for the MAV "Eagle-II". The seriously worn (reaming) portion is specifically marked with a red ellipse for the Balsa leading-edge frame (and the motor is removed in this figure.) This kind of reaming on the Balsa wood not only denotes an aging problem against good life-time of our MAVs but also reveals a certain uncommon "penalty" force resulting from the improper matching of the semi-rigid wing structures into our simple flapping mechanism.

The Knoller-Betz effect of thrust generated by means of a simply up-and-down flapping was observed in the last century (Knoller, 1909; Betz, 1912). For the conventional rigid symmetric wing with very large bending moment of inertia, the corresponding thrust force cannot react with apparent forward deformation on the whole wing structure. Additionally, the exact time location for the biggest thrust during a full flapping cycle has not been pointed out precisely by the Knoller-Betz effect. Under the constraint of the almost rigid wing frames, there seems no way but to design a complicated flapping mechanism to follow the 3-D flapping trajectory like hummingbirds (or even having the trajectory of "clap-and-pling" insects) for the artificial wingbeating vehicles. In that classical thinking of mechanism design, too much flexibility of the wing frames means the operation failure or malfunction of the flapping machines mimicking the biological gesture of natural flyers.

The design methodology in this study, on the contrary, is to use the lighter and more flexible materials as the key structures for our new version of MAVs. For instance, we tried to shorten the wingspan from 30 cm to 21.6 cm toward the miniaturization trend. The correlated body mass regulated from the scaling law of birds¹³ is no more than 10 g. For the light weight consideration, we replaced the Balsa-wood leading edge frame with fine

carbon-fiber rods. Meanwhile, the four-bar linkage transmission module is reconstructed by the electrical-discharge-wire-cutting (EDWC) of aluminum-alloy 7075. The new power transmission module made of aluminum alloy 7075 shown in Fig. 19 saves us greatly with 2 g in weight at least. This above belief or revelation from small technology is that the more miniaturized artifacts may render us with better structural stiffness and operation life time.

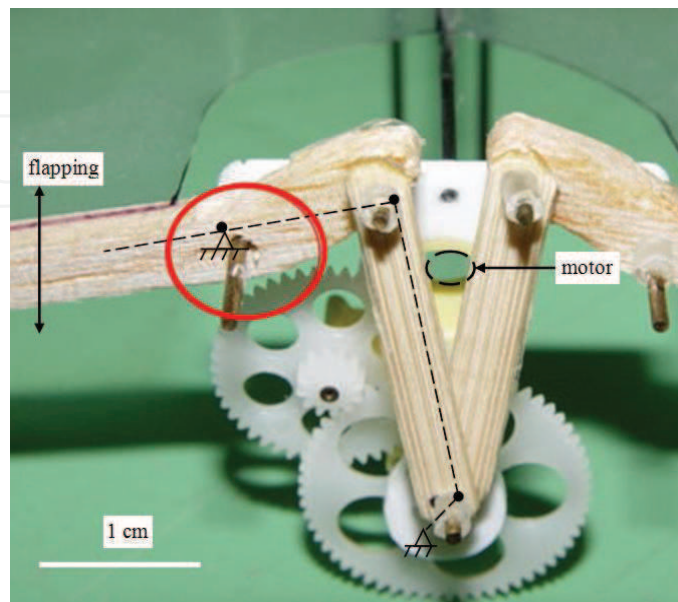


Figure 18. The four-bar (black dash line) gear transmission module for the MAV "Eagle-II". The seriously worn portion is marked with an ellipse for the Balsa leading-edge frame (and the motor is removed temporarily.)

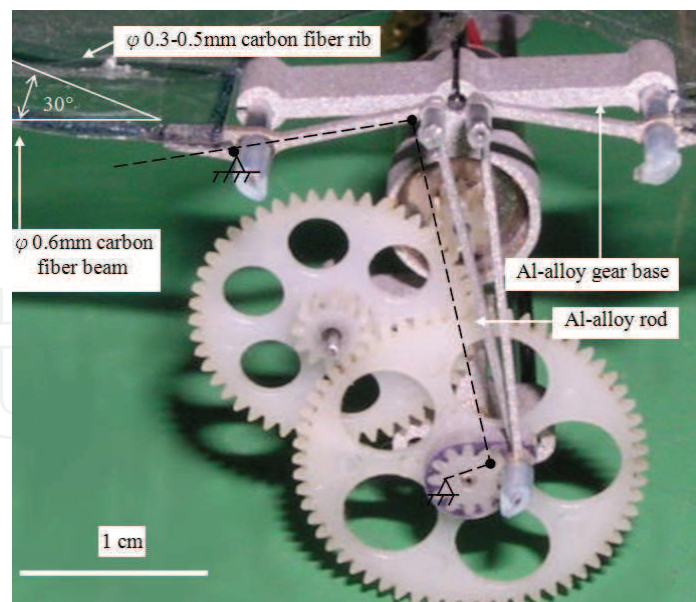


Figure 19. The weight-reduced four-bar (black dash line) gear transmission module for the MAV "Golden Snitch". The leading-edge beam is made of 0.6 mm-diameter carbon-fiber beams and aluminum-alloy bars. A rib with 30° back-swept to the leading edge beam is optionally installed. All the tiny aluminum parts were precisely manufactured by electrical-discharging-wire-cutting (EDWC)

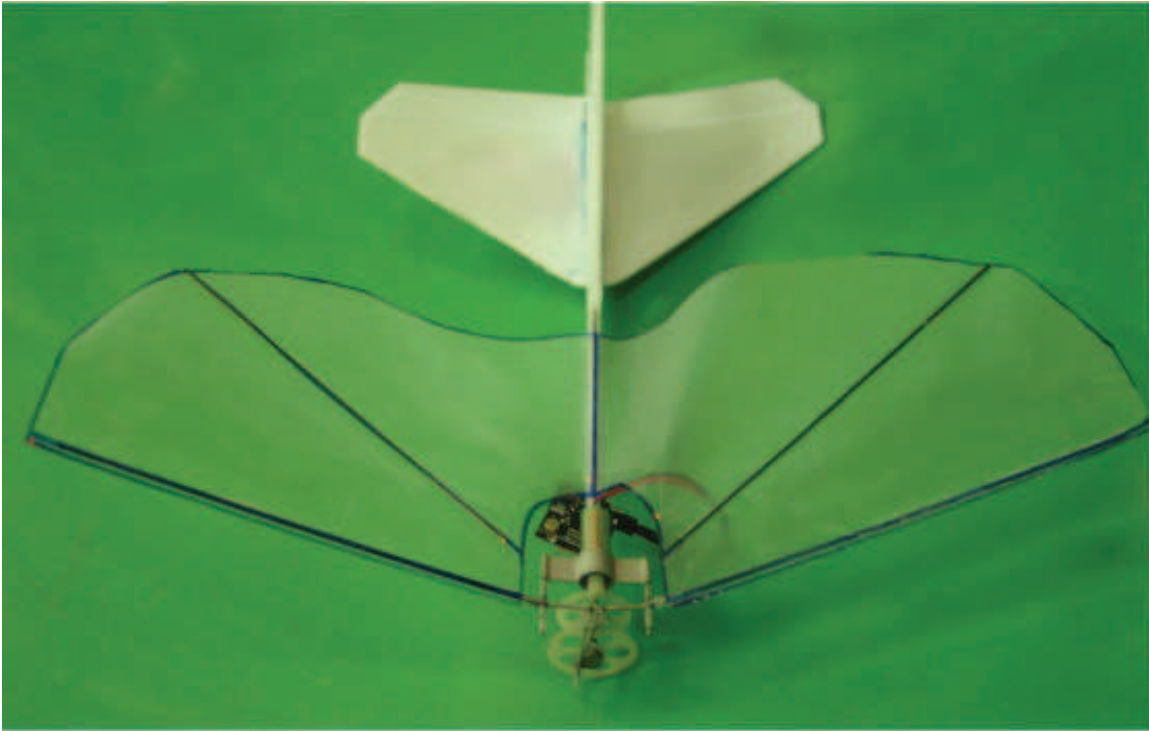
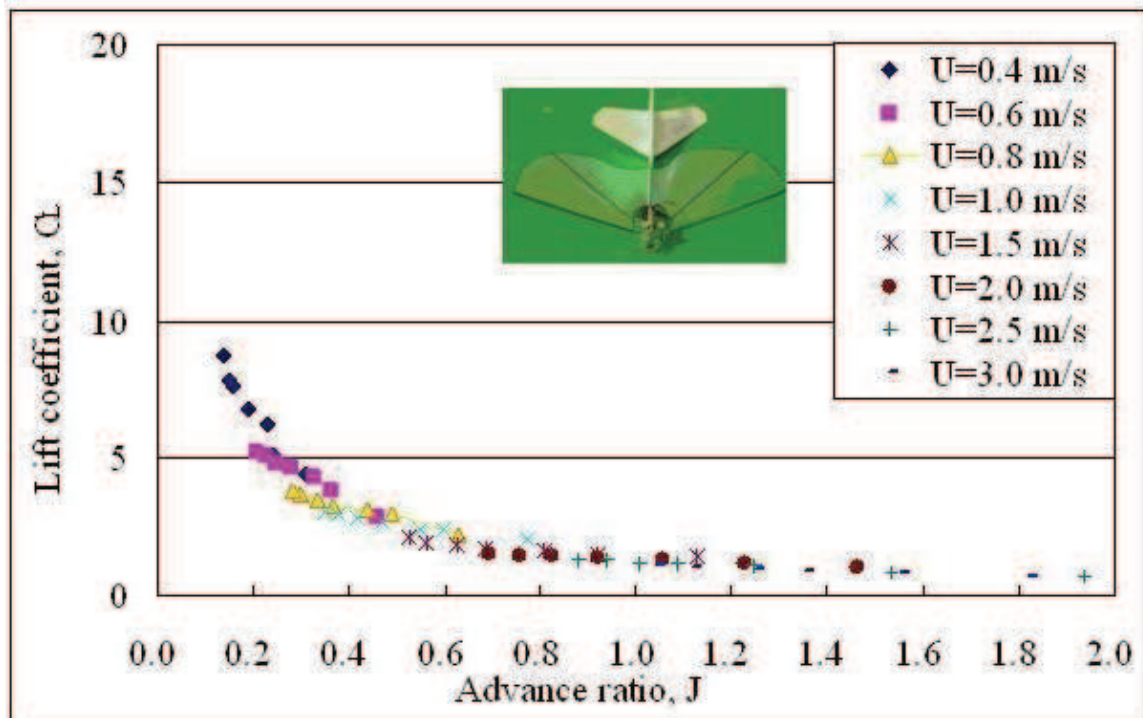
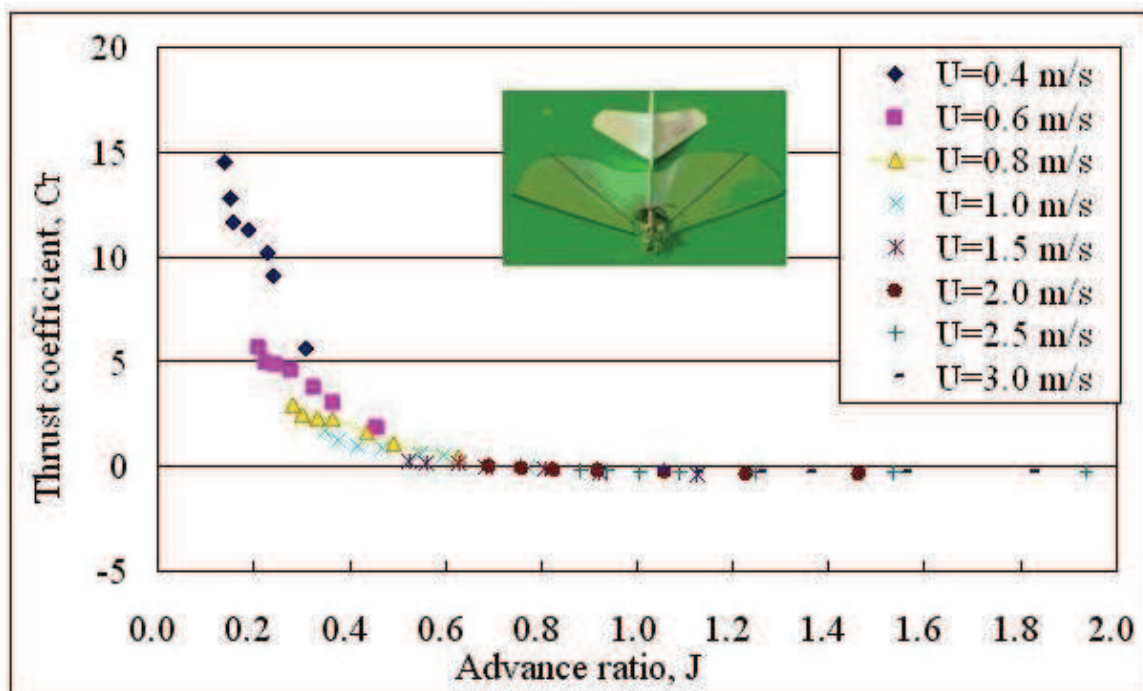


Figure 20. The completed MAV "Golden Snitch" with the carbon-fiber leading-edge beam/rib and parylene skin. A 7mm-diameter electrical motor mounted in the newly developed aluminum-alloy holder with the new transmission module is actuated by a poly-lithium battery of 30-50 mAh. The total mass including flexible wing frame, motor, gear assembly, wing, fuselage, tail, battery and receiver is only 5.9 g

We remodeled the MAV with the new flexible wing frames and the new gear transmission module mentioned above, kept reducing the total weight and wingspan, and finally obtained the modified MAV named as "Golden Snitch" (wingspan = 21.6 cm, body mass = 5.9 g) in Fig. 20. The aerodynamic coefficients versus advance ratio J for the MAV "Golden-Snitch" were measured (Fig. 21). The scheduled process of collecting data in the wind-tunnel testing is the same as the case of "Eagle-II". The new testing results of aerodynamic performance effectively improve the thrust data with 35 % increasing in magnitude and without the previous problem of unpredictable data fluctuation. The disappearance of the structure reaming on pivoting joints and the "penalty" force from the unsteady flapping prevent lots of friction loss and may benefit the real flight of our new MAVs. Furthermore, with this great decrease of friction loss in the mechanical transmission module, the wingbeat frequency of the MAV "Golden Snitch" can increase to 20 Hz or much faster than before.



(a)



(b)

Figure 21. (a) Lift coefficient C_L and (b) thrust coefficient C_T of the MAV "Golden-Snitch" versus advance ratio J corresponding to different freestream velocities U ($2b=21.6$ cm; $\phi=38.9^\circ$; $f=10.5-23.6$ Hz.)

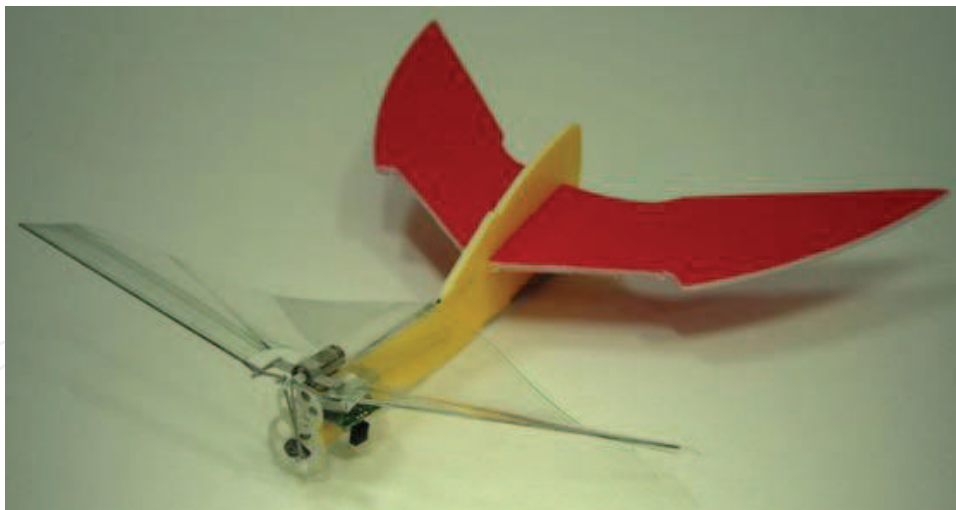
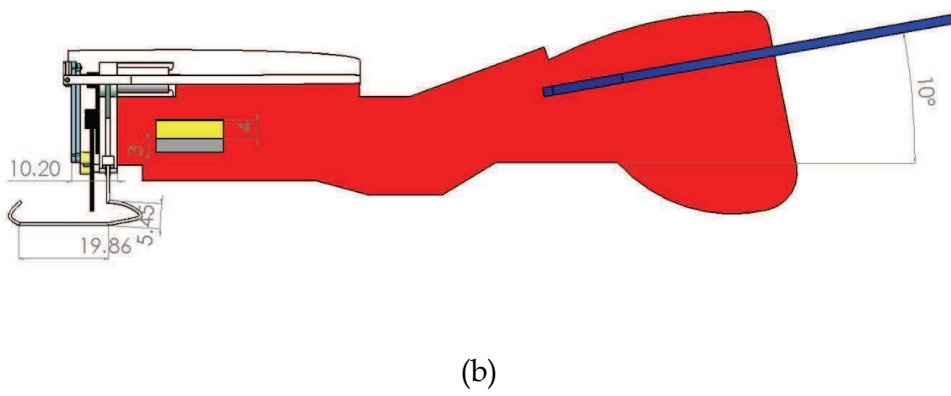
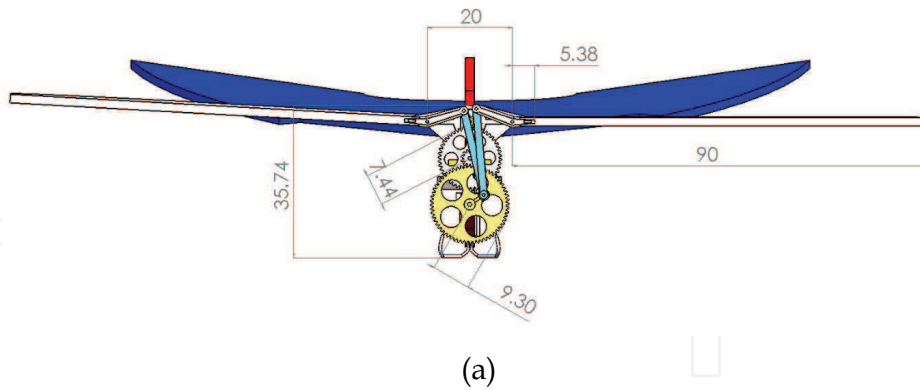


Figure 22. “Golden Snitch” with its flight endurance up to 122 s by enlarging the tail area and decreasing the corresponding tail angle: (a) the front view; (b) the side view; (c) the real plane

On the issue of evaluating the efficiency of mechanical power, the merit of removing the wing skin of our artificial MAV by the constructor can help a lot. Therefore, the flapping of the bare skeleton of wing frames can be regarded as the case for investigating the power dissipation due to the friction in the mechanical transmission mechanism. In this work, the

friction dissipation of the MAV "Eagle-II" counts 70% of the total electrical power; whereas the modified mechanism of the MAV "Golden Snitch" only consumes 45% of the total power.

The new MAV "Golden Snitch" equipped with the above new configuration and characterized with light weight and high flexibility has a far more outstanding flight performance than the semi-rigid "Eagle-II." With scarcely real-time adjustment by remote control "Golden Snitch" actually made a successful flight record of 47 s at least, breaking the 11 s record of "Eagle-II" to a great extent. Without the negative effect of side gust wind, "Golden Snitch" would like to fly roughly along the virtual barrel surface of an imaginary cylindrical column with the diameter of several meters if the horizontal tail generating negative lift is only used to stabilize the MAV. Recently, we additionally found that "Golden Snitch" can prolong its flight endurance up to 122 s by increasing the stroke angle ϕ to be 52° and enlarging the tail area like Fig. 22. In this new tail design the center of gravity of the MAV moves backwards, and high lift occurs for the positive lift contributed by the flapping wing and the horizontal tail simultaneously. It additionally shows the high-lift mode as well as the high-AOA mode of "Golden Snitch" which flies up and down along the longitudinal direction vigorously.

4.4 MAVs with flexible wing frame

Thanks to the intrinsically flexible wing structure of "Golden Snitch" herein, this MAV can fly in free flight without much energy loss in resisting against the surrounding air. And we luckily found that a streamwise vibration of the carbon-fiber leading edge is characterized by wingbeat frequency from 15.6 to 21.7 Hz for the wings with 30° -ribs. That frequency is much smaller than the natural frequency of 85 Hz for the wing structure. (It means this special vibration has no matter with the resonance of the wing frame.) By combining this induced coherent streamwise vibration of the wing frame and the vertical reciprocating flapping motion in Fig. 23, a stereo figure-of-eight flapping motion of the MAV obviously shows up and can be seen even by human naked eyesight. This is justified preliminarily by a technique of LED illumination shown in Fig. 24. This streamwise vibration of the wing frame can be originated from the forementioned Knoller-Betz effect and interpreted as a coherent forward locomotion, but the exact moment of the biggest thrust or the vibration amplitude moreover occurs at the very instants of stroke reversals, i.e., the highest and lowest points of the flapping motion. We believe that this biomimetic figure-of-eight wing tip trajectory generated by a simple flapping mechanism in flexible MAVs is first time been found and reported herein.

The ordinary video camera with 30 frames of images per second only provides too slow speed for depicting detailed viewgraphs of a full-cycle flapping kinematics in this work. The continuous blinks of the figure-of-eight trajectory of the wing tip were then taken and certificated by a high speed CCD camera (Phantom v. 4.2) for the MAV "Golden Snitch" in quiet ambient. We installed this MAV in the wind-tunnel and captured the real-time images of the flapping wings subjected to cases with and without the 30° -rib in Fig. 25. The surface morphology of the wing skin shows the wavy profile from the leading edge to trailing edge and from the wing tip to inner wing root simultaneously, which accords the supposed flexible wing design with a sinusoidal change of the leading-edge angle-of-attack. More additionally, we verified the similar phenomena of figure-of-eight flapping for the MAV "Golden Snitch" subjected to different freestream velocity which is set from 0.4 to 3.0 m/s.

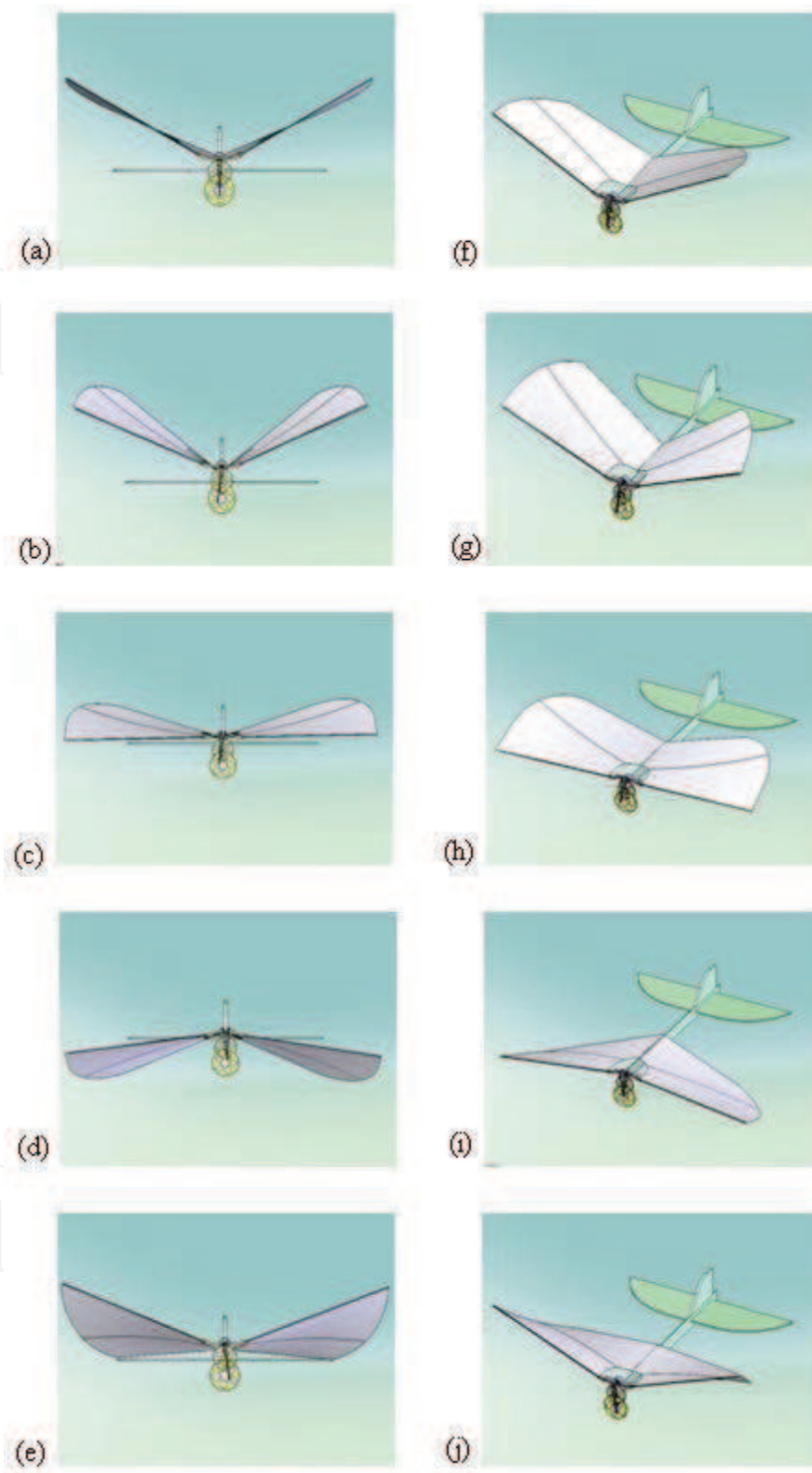


Figure 23. The supposed cartoon of the continuous full-cycle flapping motion of the MAVs with a rigid four-bar transmission module: (a) denotes the neutral position; (b) to (c) denote the downstroke; (d) to (e) denote the upstroke; the bird's-eye views from (f) to (j) are corresponding to the front side views from (a) to (e), respectively

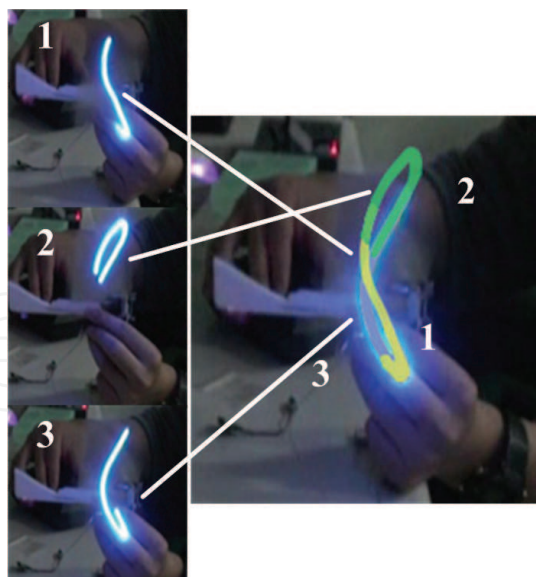


Figure 24. Wing tip trajectory by LED illumination. 1-3 are the instantaneous images of a figure-of-eight taken by a digital video. The right image combines the left 3 images

4.5 Analogous relationship in scaling laws for flapping flyer

Rather than depicting the anatomical analysis on the wing frames of flapping flyers, herein we prefer to categorize the MAV with figure-of-eight flapping into some animal groups and conventional MAVs according to their realistic wingspans and the wingbeat frequencies with respect to different body masses. Based on Norberg (Norberg, 1990), Greenewalt (Greenewalt, 1975), and Shyy's (Shyy, 1999) collecting information, the denoting spots of the MAVs "Eagle-II" (wingspan = 30 cm, body mass = 11 g, wingbeat frequency = 16Hz) and "Golden Snitch" (wingspan = 21.6 cm, body mass = 5.9 g, wingbeat frequency = 20Hz) in this work were inserted into the previous plots of wing-span versus body-mass as Fig. 26 and wingbeat-frequency versus body-mass as Fig. 27. "Eagle-II" is still allocated on the margin of conventional MAVs and small natural flyers, whereas "Golden Snitch" with figure-of-eight flapping is approaching to the characteristic region of hummingbirds. Apparently the inductive remark on this observation come to that "Golden Snitch" here has strong biomimetic relationship with hummingbirds due to the common property of figure-of-eight flapping, even though the inclined gesture of the flapping plane for these two flyers are quite different. With such an encouraging finding, the domain of MAVs marked as the shadow region in Figs. 26 and 27 extend from body mass of 11 g down to 5.9 g by this study. No matter how we followed the empirical design formulae deduced from hummingbirds, the figure-of-eight flapping is verified empirically and necessary to design a MAV which can fly successfully with wingspan less than 21.6 cm and body mass below 10 g. Subjected to this design requirement of the artificial novel figure-of-eight flapping, a flexible wing frame driven by a single DOF, four-bar linkage mechanism is provided herein as the neatest design so far as we know. In this work or the practice manner, the cross section of the leading edge carbon-fiber beam is suggested to be round, and the natural frequency of this leading edge beam should be so much larger than the wingbeat frequency without structural resonance as to sustain a successful coherent vibration out from the flap-sweeping plane due to the forward pushing by the periodic vigorous thrust.

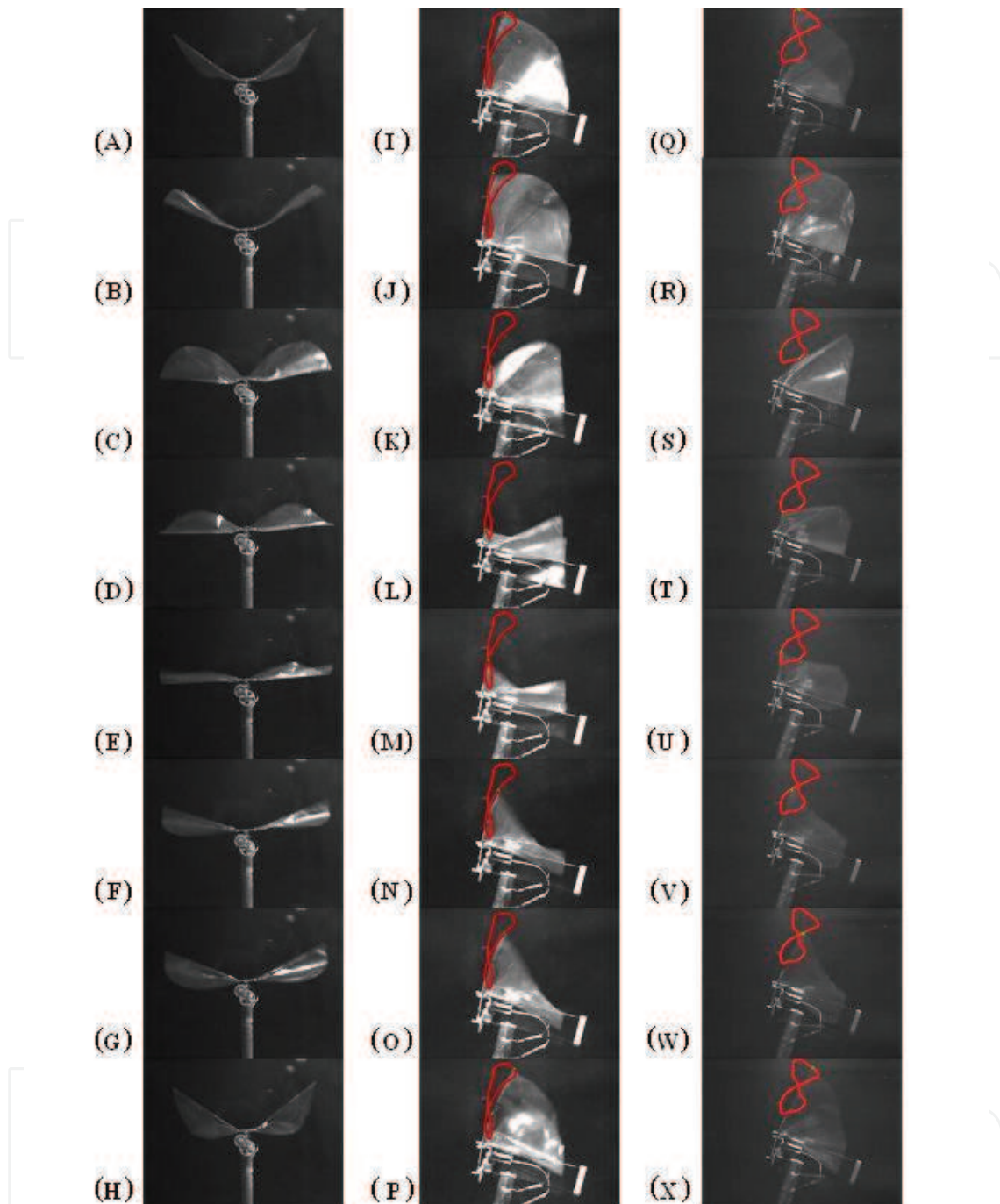


Figure 25. The continuous full-cycle blinks, taken by a high speed camera, of Golden Snitch's flapping wings. The front side views of Golden Snitch from (A) to (H) are corresponding to the side views of it without rib from (I) to (P), and to the side views of it with 30°-rib from (Q) to (X), respectively. The wingbeat frequency is 20.83 Hz. The angle of attack is 20°. The red contours added into the images show the figure-of-eight trajectories of wingtips. Even the parylene wing without the 30°-rib has the more flexible property than the stiffened 30°-rib wing, the figure-of-eight flapping still appears and the proper frequency interval for the better figure-of-eight is broader (about 9.4-25 Hz for the no-rib wing; 15.6-21.7 Hz for the stiffened 30°-rib wing.)

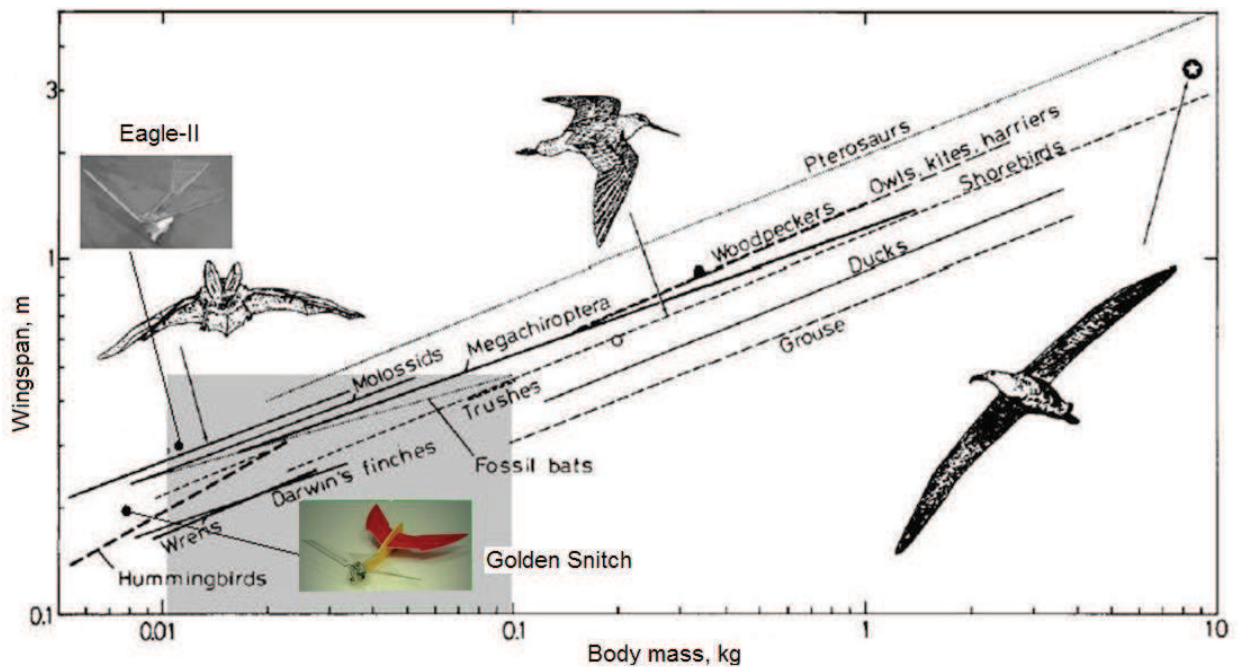


Figure 26. Wingspan plotted on logarithmic coordinates against body mass for some animal groups (Greenewalt, 1975; Norberg, 1990), conventional “shadow” region for MAVs (Shyy, 1999), and the MAVs (Eagle-II and Golden Snitch) in this chapter

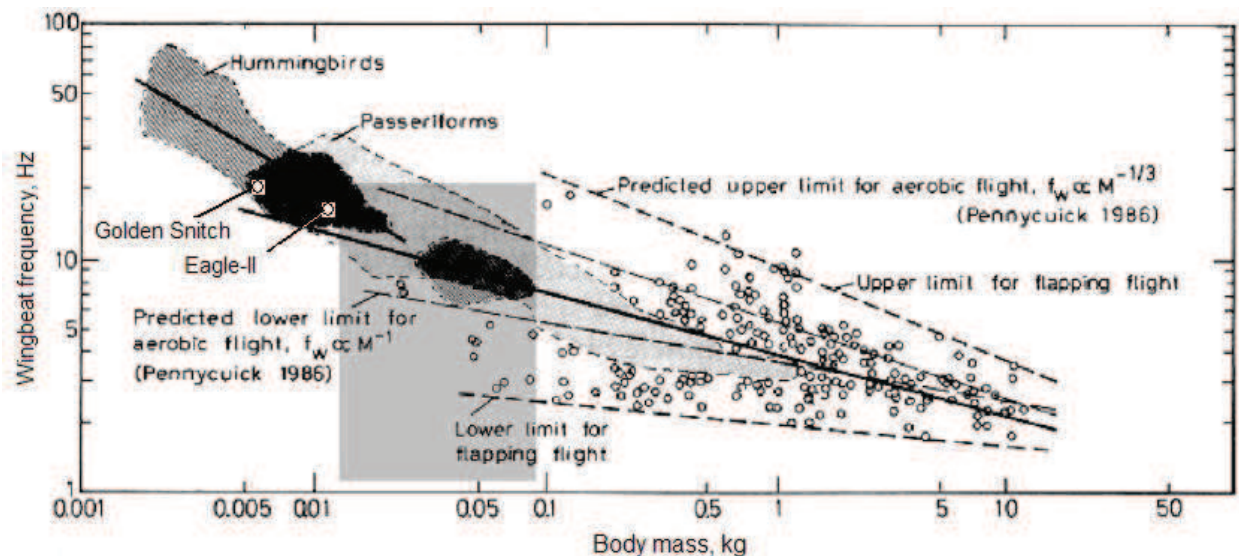


Figure 27. Wingbeat frequency (or flapping frequency) versus body mass for some animal groups (Greenewalt, 1975; Norberg, 1990), conventional “shadow” region for MAVs (Shyy, 1999), and the MAVs (Eagle-II and Golden Snitch) in this chapter

5. CONCLUSION

This study presents a smart wing with PVDF-parylene composite wing by MEMS fabricating process and a four-bar linkage transmission system with variable phase lags of the flapping wings. The signals from the PVDF film and the load-cell are acquired simultaneously and the curves are quite similar. This result demonstrates that the smart

PVDF skin has the promising capability to monitor aerodynamic information of flapping in the future. In the wind-tunnel tests, the collected data has a phase lag between the PVDF and load-cell curves due to the design of asymmetric flapping movement. By a superimposing method, the “pseudo” PVDF curve has higher similarity to the lift signals. The smart PVDF-parylene composite wing and the superimposing method can help to design a micro MAV with ideal aerodynamic characteristic by changing the phase lag between the two flapping wings through fine tuning of the mechanism linkages.

The performances of flapping wings are also studied in this chapter. The lift force increases with the square of the wind speed in the non-flapping mode. In the unsteady state or the flapping mode of our MAVs, the two-wing configuration has greater superiority in terms of aerodynamic performance than the single wing configuration. It is apparent that stiffness of flapping wing plays an important role in producing lift and trust forces. The first generation MAV which has wingspan of 30 cm, including one commercial lithium battery herein has a total weight less than 11 grams and it has a successful flight of more than 40 meters by wireless remote control.

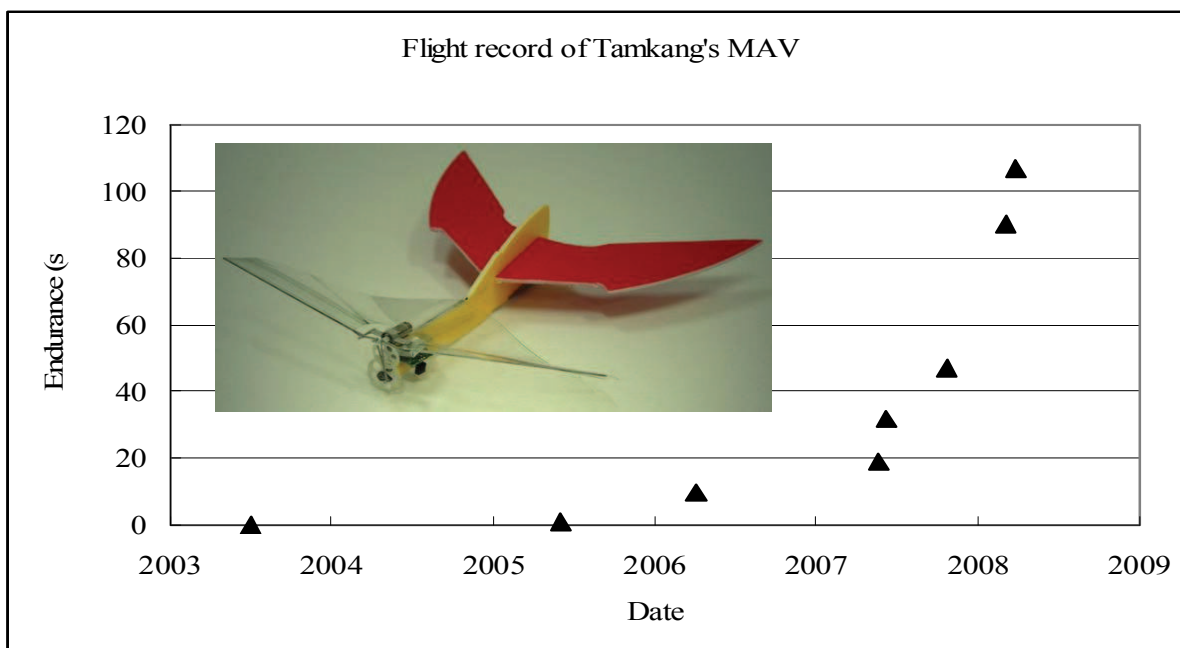


Figure 28. Flight record of MAVs developed in Tamkang University

Additionally, the passive design aspect of improving the performance of the wing frames for flapping MAVs “Eagle-II” and “Golden Snitch” in this chapter tends to provide a simpler flying platform with moderate gear-transmission module but to produce bountiful and interesting phenomena deserving furthermore biomimetic study. With the help of a high-speed camera, the figure-of-eight trajectories of the wing tips of “Golden Snitch” were verified by their proper function of the carbon-fiber wing frames and the parylene wing skin. The unsteady lift data and the highly enhanced thrusting locomotion acquired from the wind-tunnel testing did great contribution to the successful flight of our MAVs, even the implied unsteady flow mechanism still needs more theoretical explanations and more supporting evidences. This work also removed the technical barrier against the designers in making complicated multi-DOF actuating mechanisms for generating figure-of-eight flapping. Finally, with the advantage of light-weight and size miniaturization, we effectively

extend the existing domain of MAVs and created new flight record depicted in Fig. 28. We believe this neatest design methodology for flapping MAVs will be promising in practice, and the correlated flow visualization of the figure-of-eight or the theoretical investigation of the solid-fluidic (aero-elastic) interaction deserve follow-up attentions.

6. ACKNOWLEDGEMENT

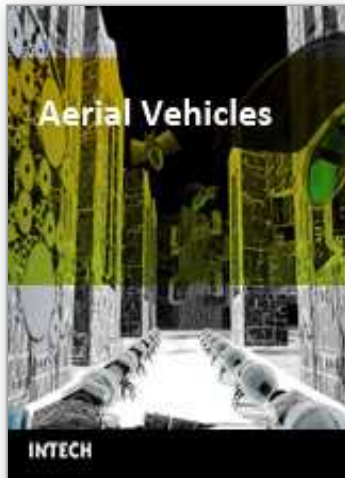
We would like to thank the financial support from National Science Council of Taiwan by the project numbers of NSC-93-2212-E-032-012, 94-2212-E-032-012, 96-2221-E-032-013, 96-2221-E-032-014, 97-2628-E032-015, 97-2221-E-032-016 and the experimental helps from Dr. C.-K. Hsu, Prof. S.-W. Kang, Prof. F.-Y. Hsiao, Mr. H.-M. Shih, Mr. M.-W. Gao, Dr. W.-C. Wei, Mr. C.-Y. Kao, and Mr. J.-W. Liao of Tamkang University. The discussions with Prof. Y.-C. Tai of Caltech, Prof. W.-P. Shih, Prof. A.-B. Wang of National Taiwan University, Prof. Y.-K. Shen of Taipei Medical University, and Prof. J.-M. Miao of National Defense University, are also highly acknowledged.

7. REFERENCES

- Ashley, S. (1998). Palm-size spy plane, *The American Society of Mechanical Engineers*, February, 74.
- Betz, A. (1912). Ein beitrage zur erklärung des segelfluges, *Zeitschrift für Flugtechnik und Motorluftschiffahrt*, 3, 269-272.
- Barrett, R., McMurtry, R., Vos, R., Tiso, P., and De Breuker, R. (2005). Post-buckled precompressed (PBP) elements: a new class of flight control actuators enhancing high-speed autonomous VTOL MAVs, *Proceedings of SPIE - The International Society for Optical Engineering*, Vol. 5762, San Diego, USA, May, 7-9, pp. 111-122.
- Banala, S.K. and Agrawal, S.K. (2005). Design and optimization of a mechanism for out-of-plane insect winglike motion with twist, *Journal of Mechanical Design/ Transactions of the ASME*, 127(4), 841-844.
- Cloupeau, M. (1979). Direct measurements of instantaneous lift in desert locust: comparison with Jensen's experiments on detached wings, *J. Exp. Biol.*, 80, 1-15.
- Chanute, O. (1894). *Progress in Flying Machines*, Dover Publications, Inc.
- Dickinson, M.H. and Götz, K. (1996). The wake dynamics and flight forces of the fruit fly *Drosophila melanogaster*, *J. Exp. Biol.*, 199(99), 2085-2104.
- Greenewalt, C.H. (1975). The flight of birds, *Trans. Am. Philos. Soc.*, 65, 1-67.
- Ho, S., Nassef, H., Pornsinsirak, T.N., and Tai, Y.C. (2003). Unsteady aerodynamics and flow control for flapping wing flyers, *Progress in Aerospace Science*, 39, 635-681.
- Hollick, F.S.J. (1940). The flight of the dipterous fly *Muscina stabulans* fallen, *Phil. Trans.*, B 230, 357-90.
- Jensen, M. (1956). Biology and physics of locust flight. III. The aerodynamics of locust flight, *Philosophical Transactions of the Royal Society of London, Series B, Biological Sciences*, 239(667), 511-552.
- Jones, K.D., Bradshaw, C.J., Papadopoulos, J., and Platzer, M.F. (2005). Bio-inspired design of flapping-wing micro aerial vehicles, *Aeronautical Journal*, 109(1098), 385-393.
- Knoller, R. (1909). Die Gesetze des luftwiderstands, *Flug-und Motortechnik (Wien)*, 3(21), 1-7.
- Liu, C. (2006). *Foundations of MEMS*, Pearson/Prentice Hall, 1st ed, p.256.

- McIntosh, S.H., Agrawal, S.K., and Khan, Z. (2006). Design of a mechanism for biaxial rotation of a wing for a hovering vehicle, *IEEE/ASME Transactions on Mechatronics*, 11(2), 145-153.
- Norberg, U.M. (1990). *Vertebrate Flight: Mechanics, Physiology, Morphology, Ecology and Evolution*, Springer-Verlag, New York, Chapters 2, 8, 9, 10.
- Pornsirirak, T.N. et al. (2001). Titanium-alloy MEMS wing technology for a micro aerial vehicle application, *Sensors and Actuators A: Physical*, 89, 95-103.
- Pornsirirak, T.N. et al. (2002). Flexible parylene-valved skin for adaptive flow control, Proceedings of 15th IEEE MEMS conference, Las Vegas, USA, pp. 101-104.
- Shyy, W., Berg, M., and Ljungqvist, D. (1999). Flapping and flexible wings for biological and micro air vehicles, *Progress in Aerospace Sciences*, 35, 455-505.
- Sitti, M. (2001). PZT actuated four-bar mechanism with two flexible links for micromechanical flying insect thorax, Proceedings of the IEEE Robotics and Automation Conference, Korea, pp. 3893-3900.
- Weller, E.J. (1983). *Nontraditional Machining Processes*, 2nd Edition, The Society of Manufacturing Engineers.
- Yang, L.J., Hsu, C.K., Ho, J.Y. and Feng, C.K. (2007). Flapping wings with PVDF sensors to modify the aerodynamic forces of a micro aerial vehicle, *Sensors and Actuators A: Physical*, 139, 95-103.
- Żbikowski, R., Galin'ski, C., and Pedersen, C.B. (2005). Four-bar linkage mechanism for insectlike flapping wings in hover: concept and an outline of its realization, *Journal of Mechanical Design/ Transactions of the ASME*, 127(4), 817-824.
- Żbikowski, R. and Galin'ski, C. (2005). Insect-like flapping wing mechanism based on a double spherical Scotch yoke, *Journal of the Royal Society Interface*, 2, 223-235.

IntechOpen



Aerial Vehicles

Edited by Thanh Mung Lam

ISBN 978-953-7619-41-1

Hard cover, 320 pages

Publisher InTech

Published online 01, January, 2009

Published in print edition January, 2009

This book contains 35 chapters written by experts in developing techniques for making aerial vehicles more intelligent, more reliable, more flexible in use, and safer in operation. It will also serve as an inspiration for further improvement of the design and application of aerial vehicles. The advanced techniques and research described here may also be applicable to other high-tech areas such as robotics, avionics, vetronics, and space.

How to reference

In order to correctly reference this scholarly work, feel free to copy and paste the following:

Lung-Jieh Yang (2009). Flapping Wings with Micro Sensors and Flexible Framework to Modify the Aerodynamic Forces of a Micro Aerial Vehicle (MAV), *Aerial Vehicles*, Thanh Mung Lam (Ed.), ISBN: 978-953-7619-41-1, InTech, Available from:

http://www.intechopen.com/books/aerial_vehicles/flapping_wings_with_micro_sensors_and_flexible_framework_to_modify_the_aerodynamic_forces_of_a_micro

INTECH

open science | open minds

InTech Europe

University Campus STeP Ri
Slavka Krautzeka 83/A
51000 Rijeka, Croatia
Phone: +385 (51) 770 447
Fax: +385 (51) 686 166
www.intechopen.com

InTech China

Unit 405, Office Block, Hotel Equatorial Shanghai
No.65, Yan An Road (West), Shanghai, 200040, China
中国上海市延安西路65号上海国际贵都大饭店办公楼405单元
Phone: +86-21-62489820
Fax: +86-21-62489821

© 2009 The Author(s). Licensee IntechOpen. This chapter is distributed under the terms of the [Creative Commons Attribution-NonCommercial-ShareAlike-3.0 License](https://creativecommons.org/licenses/by-nc-sa/3.0/), which permits use, distribution and reproduction for non-commercial purposes, provided the original is properly cited and derivative works building on this content are distributed under the same license.

IntechOpen

IntechOpen